

# Heavy flavor production off protons and in a nuclear environment

B. Z. Kopeliovich<sup>1,2,3</sup> and J. Raufeisen<sup>4</sup>

<sup>1</sup> Max-Planck Institut für Kernphysik, Postfach 103980, 69029 Heidelberg, Germany

<sup>2</sup> Institut für Theoretische Physik der Universität, 93040 Regensburg, Germany

<sup>3</sup> Joint Institute for Nuclear Research, Dubna, 141980 Moscow Region, Russia

<sup>4</sup> Los Alamos National Laboratory, MS H846, Los Alamos, NM 87545, USA

**Abstract.** These lectures present an overview of the current status of the QCD based phenomenology for open and hidden heavy flavor production at high energies. A unified description based on the light-cone color-dipole approach is employed in all cases. A good agreement with available data is achieved without fitting to the data to be explained, and nontrivial predictions for future experiments are made. The key phenomena under discussion are: (i) formation of the wave function of a heavy quarkonium; (ii) quantum interference and coherence length effects; (iii) Landau-Pomeranchuk suppression of gluon radiation leading to gluon shadowing and nuclear suppression of heavy flavors; (iv) higher twist shadowing related to the finite size of heavy quark dipoles; (v) higher twist corrections to the leading twist gluon shadowing making it process dependent.

## 1 Introduction

Reactions in which heavy flavors are produced involve a hard scale that allows one to employ perturbative QCD (pQCD). In particular, production off nuclei has always been an important topic in heavy quark physics. On the one hand, interest in this field is stimulated by demand to provide a proper interpretation for available and forthcoming data, especially from heavy ion collisions. On the other hand, nuclei have been traditionally employed as an analyzer for the dynamics and time scales of hadronic interactions.

In these lectures, we shall review the color dipole formulation of heavy flavor production, which was developed in [1–4]. The dipole approach to heavy flavor production expresses the cross section for production of open or hidden heavy flavor in terms of the cross section for scattering a color neutral quark-antiquark ( $q\bar{q}$ ) pair off a nucleon. This approach is motivated by the need for a theoretical framework for the description of nuclear effects. Its main distinction from the conventional parton model is the possibility to actually calculate nuclear effects in the dipole formulation, rather than absorbing them into the initial conditions. In addition, the dipole approach is not restricted to the leading twist approximation. This is especially important for nuclear effects in  $J/\psi$  production, which are dominated by higher twists. Another advantage of the dipole approach is that it correctly describes the absolute normalization of cross sections in different processes, without introducing an arbitrary overall normalization factor

(“ $K$ -factor”) [5,6]. However, the dipole approach is applicable only in the kinematical domain, where the heavy quark mass  $m_Q$  is much smaller than the center of mass ( $cm.$ ) energy  $\sqrt{s}$ . The latter condition is fulfilled for charm production at the BNL Relativistic Heavy Ion Collider (RHIC) and for both, charm and bottom production, at the CERN Large Hadron Collider (LHC).

An alternative approach to heavy quark production that is designed especially for high energies and which is able to describe nuclear effects is desirable for a variety of reasons. At low  $x$ , the heavy quark pair is produced over large longitudinal distances, which can exceed the radius of a large nucleus by orders of magnitude. Indeed, even though the matrix element of a hard process is dominated by short distances, of the order of the inverse of the hard scale, the cross section of that process also depends on the phase space element. Due to gluon radiation, the latter becomes very large at high energies, and it is still a challenge how to resum the corresponding low- $x$  logarithms. The dipole formulation allows for a simple phenomenological recipe to include these low- $x$  logs. The large length scale in the problem leads to pronounced nuclear effects, giving one the possibility to use the nuclear medium as microscopic detectors to study the space-time evolution of heavy flavor production.

In addition, heavy quark production is of particular interest, because this process directly probes the gluon distributions of the colliding particles. Note that at the tremendous center of mass energies of RHIC and LHC, charm (and at LHC also bottom) decays will dominate the dilepton continuum [7]. Thus, a measurement of the heavy quark production cross section at RHIC and LHC will be relatively easy to accomplish and can yield invaluable information about the (nuclear) gluon density [8]. It is expected that at very low  $x$ , the growth of the gluon density will be slowed down by nonlinear terms in the QCD evolution equations [9]. The onset of this non-linear regime is controlled by the so-called saturation scale  $Q_s(x, A)$ , which is already of order of the charm quark mass at RHIC and LHC energies. Moreover,  $Q_s(x, A) \propto A^{1/3}$  ( $A$  is the atomic mass of the nucleus), so that one can expect sizable higher twist corrections in  $AA$  collisions [4]. Note that saturation will lead to a breakdown of the twist expansion, since one cannot conclude any more that terms suppressed by powers of the heavy quark mass  $m_Q$  are small,  $Q_s^n(x, A)/m_Q^n \in O(1)$  for any  $n$  [10]. Saturation effects are most naturally described in the dipole picture.

The most prominent motivation for a theoretical investigation of nuclear effects in heavy flavor production is perhaps the experimentally observed suppression of  $J/\psi$  mesons in nuclear collisions, see Ref. [11] for a review. Suppression of  $J/\psi$  production in nucleus-nucleus ( $AA$ ) collisions has been proposed as signal of quark-gluon plasma (QGP) formation [12]. There are however several “mundane” nuclear effects that also lead to  $J/\psi$  suppression, such as gluon shadowing, final state absorption and breakup due to interactions with comovers. This issue has been widely and controversially discussed in the literature, and one clearly needs a reliable theoretical description of all these effects, before definite conclusions about any non-standard dynamics in heavy ion collisions can be drawn. Since the creation and study of the QGP is the main physics motivation for

RHIC, the theoretical investigation of nuclear effects in  $J/\psi$  production is at the heart of the RHIC heavy ion program. Note that the production mechanism for heavy quarkonia itself is poorly understood, even in proton-proton ( $pp$ ) collisions. However, since heavy flavors can be produced in many different reactions, and one may hope that a detailed experimental and theoretical study of quarkonium production in different environments and over a wide kinematical range will eventually clarify the underlying production mechanism.

## 2 The foundations of the color dipole approach to high energy scattering

It was first realized in [13] that at high energies color dipoles with a well defined transverse separation are the eigenstates of interaction at, i.e. can experience only diagonal transitions when interacting diffractively with a target. The eigenvalues of the amplitude operator are related to the cross section  $\sigma_{q\bar{q}}(r)$  of interaction of a  $q\bar{q}$  dipole with a nucleon. This dipole cross section is a universal, flavor independent quantity which depends only on transverse  $q\bar{q}$  separation. Then, the total hadron (meson) nucleon cross section can be presented in a factorized form,

$$\sigma_{tot}^{hN} = \int d^2r |\Psi_{q\bar{q}}^h(\mathbf{r})|^2 \sigma_{q\bar{q}}(r) , \quad (1)$$

where  $\Psi_{q\bar{q}}^h(\mathbf{r})$  is the light-cone wave function of the  $q\bar{q}$  component of the hadron. It was assumed in [13] that  $|\Psi_{q\bar{q}}^h(\mathbf{r})|^2$  is integrated over longitudinal coordinate.

One of the advantages of this approach is simplicity of calculation of the effects of multiple interactions which have the eikonal form (exact for eigenstates),

$$\sigma_{tot}^{hA} = 2 \int d^2b \int d^2r |\Psi_{q\bar{q}}^h(\mathbf{r})|^2 \left\{ 1 - \exp \left[ -\frac{1}{2} \sigma_{q\bar{q}}(r) T_A(b) \right] \right\} , \quad (2)$$

where  $T_A(b)$  is the nuclear thickness function which depends on impact parameter  $\mathbf{b}$ .

Later the energy dependence of the dipole cross section was taken into account [14], and was found that one can apply the same color-dipole formalism to variety of QCD processes, including radiation [15]. Here we review this approach applied to production of heavy flavors.

The simplest example for heavy flavor production is open heavy quark production in deep inelastic scattering (DIS) off a proton, which can be measured at the DESY  $ep$  collider HERA. We use this example to explain the basic ideas underlying the color dipole approach to high energy scattering.

The dipole approach is formulated in the target rest frame, where DIS looks like pair creation in the gluon field of the target, see Fig. 1. For further simplification, we consider only the case of a longitudinally polarized  $\gamma^*$  with virtuality  $Q^2$  in this section, since the transverse polarization does not contain any qualitatively new physics. A straightforward calculation of the two Feynman diagrams

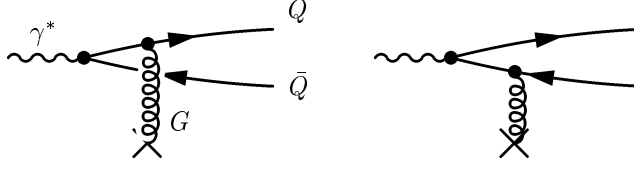


**Fig. 1.** Perturbative QCD graphs for heavy quark ( $Q\bar{Q}$ ) production in DIS. The virtual photon ( $\gamma^*$ ) fluctuates into a (virtual)  $Q\bar{Q}$ -pair far before the target. The interaction with the target, which is denoted by gluon ( $G$ ) exchange, can put this fluctuation on mass shell.

in Fig. 1 yields for the transverse momentum ( $\kappa_\perp$ ) distribution of the heavy quark [16],

$$\frac{d\sigma(\gamma_L^* p \rightarrow \{Q\bar{Q}\}X)}{d^2\kappa_\perp} = \frac{4\alpha_{\text{em}}\alpha_s e_Q^2 Q^2}{\pi} \int d\alpha \alpha^2 (1-\alpha)^2 \times \int \frac{d^2k_T}{k_T^2} \left( \frac{1}{\kappa_\perp^2 + \varepsilon^2} - \frac{1}{(\kappa_\perp - \mathbf{k}_T)^2 + \varepsilon^2} \right)^2 \mathcal{F}(x, k_T^2) \quad (3)$$

where  $\alpha$  is the light-cone momentum fraction of the heavy quark and  $\varepsilon^2 = \alpha(1-\alpha)Q^2 + m_Q^2$ . The quark electric charge is denoted by  $e_Q$ ;  $\alpha_{\text{em}} = 1/137$  and  $\alpha_s$  are the electromagnetic and the strong coupling constants, respectively. The  $Q\bar{Q}$ -pair exchanges a gluon with transverse momentum  $\mathbf{k}_T$  with the target. The latter is characterized by the unintegrated gluon density  $\mathcal{F}(x, k_T^2)$ . Note that Eq. (3) is also valid for light flavors.

In the dipole approach, a mixed representation is employed, that treats the longitudinal ( $\gamma^*$ ) direction in momentum space, but the two transverse directions are described in coordinate (*i.e.* impact parameter) space. With help of the relation

$$\frac{1}{\kappa_\perp^2 + \varepsilon^2} = \int \frac{d^2r}{2\pi} K_0(\varepsilon r) e^{-i\kappa_\perp \cdot \mathbf{r}}, \quad (4)$$

where  $K_0$  is the zeroth order MacDonal function [17], one can Fourier transform Eq. (3) into impact parameter space,

$$\frac{d\sigma(\gamma_L^* p \rightarrow \{Q\bar{Q}\}X)}{d^2\kappa_\perp} = \frac{1}{(2\pi)^2} \int d\alpha \int d^2r_1 d^2r_2 e^{i\kappa_\perp \cdot (\mathbf{r}_1 - \mathbf{r}_2)} \times \Psi_{\gamma^* \rightarrow Q\bar{Q}}(\alpha, \mathbf{r}_1) \Psi_{\gamma^* \rightarrow Q\bar{Q}}^*(\alpha, \mathbf{r}_2) \times \frac{1}{2} \left\{ \sigma_{q\bar{q}}(r_1, x) + \sigma_{q\bar{q}}(r_2, x) - \sigma_{q\bar{q}}(\mathbf{r}_1 - \mathbf{r}_2, x) \right\} \quad (5)$$

Since the  $\mathbf{r}_i$  are conjugate variables to  $\kappa_\perp$ , one can interpret  $\mathbf{r}_1$  as the transverse size of the  $Q\bar{Q}$ -pair in the amplitude and  $\mathbf{r}_2$  as the size of the pair in the complex conjugate amplitude. An expression similar to Eq. (5) was also obtained in Ref. [18].

The light-cone (LC) wavefunctions for longitudinal ( $L$ ) and for transverse ( $T$ ) photons are given by

$$\begin{aligned} \Psi_{\gamma^* \rightarrow Q\bar{Q}}^L(\alpha, \mathbf{r}_1) \Psi_{\gamma^* \rightarrow Q\bar{Q}}^{*L}(\alpha, \mathbf{r}_2) &= \frac{6\alpha_{\text{em}} e_Q^2}{(2\pi)^2} 4Q^2 \alpha^2 (1-\alpha)^2 K_0(\varepsilon r_1) K_0(\varepsilon r_2) \quad (6) \\ \Psi_{\gamma^* \rightarrow Q\bar{Q}}^T(\alpha, \mathbf{r}_1) \Psi_{\gamma^* \rightarrow Q\bar{Q}}^{*T}(\alpha, \mathbf{r}_2) &= \frac{6\alpha_{\text{em}} e_Q^2}{(2\pi)^2} \left\{ m_Q^2 K_0(\varepsilon r_1) K_0(\varepsilon r_2) \right. \\ &\quad \left. + \left[ \alpha^2 + (1-\alpha)^2 \right] \varepsilon^2 \frac{\mathbf{r}_1 \cdot \mathbf{r}_2}{r_1 r_2} K_1(\varepsilon r_1) K_1(\varepsilon r_2) \right\} \quad (7) \end{aligned}$$

The concept of LC wavefunction of a photon was first introduced in Refs. [19,20]. These wavefunctions are simply the  $\gamma^* \rightarrow Q\bar{Q}$  vertex times the Feynman propagator for the quark line in Fig. 1, and can therefore be calculated in perturbation theory.

The flavor independent dipole cross section  $\sigma_{q\bar{q}}$  in Eq. (5) carries all the information about the target. It is related to the unintegrated gluon density by [21]

$$\sigma_{q\bar{q}}(r, x) = \frac{4\pi}{3} \int \frac{d^2 k_T}{k_T^2} \alpha_s \mathcal{F}(x, k_T) \{1 - e^{-i\mathbf{k}_T \cdot \mathbf{r}}\}. \quad (8)$$

The color screening factor in the curly brackets in Eq. (8) ensures that  $\sigma_{q\bar{q}}(r, x)$  vanishes  $\propto r^2$  (modulo logs) at small separations. This seminal property of the dipole cross section is known as *color transparency* [13,22,23]. The dipole cross section cannot be calculated from first principles, but has to be determined from experimental data, see sect. 3. In principle, the energy, *i.e.*  $x$ , dependence of  $\sigma_{q\bar{q}}$  could be calculated in perturbative QCD. This has been attempted in the generalized BFKL approach of Nikolaev and Zakharov, see *e.g.* [21], by resumming higher orders in perturbation theory. However, the widely discussed next-to-leading order (NLO) corrections to the BFKL equation [24,25] has left the theory of low- $x$  resummation in an unclear state. We shall account for higher order effects by using a phenomenological parameterization of the dipole cross section.

In the high energy limit, one can neglect the dependence of the gluon momentum fraction  $x$  on  $\kappa_\perp$  and integrate Eq. (5) over  $\kappa_\perp$  from 0 to  $\infty$ . One then obtains a particularly simple formula for the total cross section,

$$\sigma_{\text{tot}}(\gamma^* p \rightarrow \{Q\bar{Q}\}X) = \sum_{T,L} \int d\alpha \int d^2 r \left| \Psi_{\gamma^* \rightarrow Q\bar{Q}}^{T,L}(\alpha, \mathbf{r}_1) \right|^2 \sigma_{q\bar{q}}(r, x). \quad (9)$$

It was argued in Ref. [26] that the dipole formulation is valid only in the leading  $\log(x)$  approximation where Eq. (9) holds. Note however that Eq. (5) does not rely on any high energy approximation and is exactly equivalent to the  $k_T$ -factorized expression Eq. (3).

Eq. (9) has an illustrative interpretation, which is the key to calculating nuclear effects in the dipole approach: The total cross section can be written in factorized form in impact parameter space, because partonic configurations

with fixed transverse separations are eigenstates of the interaction [13,27], *i.e.* of the  $T$  matrix restricted to diffractive processes. Intuitively, the transverse size is frozen during the entire interaction because of time dilation. In the dipole approach, the projectile is expanded in these eigenstates,

$$|\gamma^*\rangle = \sum_k c_k^{\gamma^*} |\psi_k\rangle, \quad (10)$$

with

$$-iT|\psi_k\rangle = \sigma_k |\psi_k\rangle. \quad (11)$$

Each eigenstate scatters independently off the target. According to the optical theorem, the total cross section is then given by

$$\sigma_{\text{tot}} = \text{Im}\langle\gamma^*|T|\gamma^*\rangle = \sum_k |c_k^{\gamma^*}|^2 \sigma_k. \quad (12)$$

Comparing this expression, Eq. (12), with Eq. (3), one can identify  $\sigma_{q\bar{q}}(r, x)$  as an eigenvalue of the  $T$ -matrix and the coefficients  $c_k^{\gamma^*}$  as LC wavefunctions. The summation over the index  $k$  is replaced by the integrals over  $\alpha$  and  $r$ .

Knowing the eigenstates of the interaction is a great advantage in calculating multiple scattering effects in nuclear collisions. Note however that the quark-antiquark pair is only the lowest Fock component of the virtual photon. There are also higher Fock states containing gluons, which are not taken into account by these simple considerations. These gluons cause the  $x$ -dependence of the dipole cross section and will be included in a phenomenological way, see sect. 3. In addition, at lower energies color dipoles are no longer exact eigenstates. A dipole of size  $r_1$  may evolve into a dipole of a different size  $r_2$ . This can be calculated from Eq. (5).

### 3 The phenomenological dipole cross section

The total cross sections for all hadrons and (virtual) photons are known to rise with energy. It is obvious that the energy dependence cannot originate from the hadronic wave functions, but only from the dipole cross section. In the approximation of two-gluon exchange used in [13] the dipole cross section is constant, the energy dependence originates from higher order corrections related to gluon radiation. Since no reliable way is known so far to sum up higher order corrections, especially in the semihard regime, we resort to phenomenology and employ a parameterization of  $\sigma_{q\bar{q}}(r, x)$ .

Few such parameterizations are available in the literature, we choose two of them which are simple, but quite successful in describing data and denote them by the initials of the authors as ‘‘GBW’’ [28] and ‘‘KST’’ [29].

We have

$$\begin{aligned} \text{‘‘GBW’’:} \quad \sigma_{q\bar{q}}(r, x) &= 23.03 \left[ 1 - e^{-r^2/r_0^2(x)} \right] \text{ mb} , & (13) \\ r_0(x) &= 0.4 \left( \frac{x}{x_0} \right)^{0.144} \text{ fm} , \end{aligned}$$

where  $x_0 = 3.04 \cdot 10^{-4}$ . The proton structure function calculated with this parameterization fits very well all available data at small  $x$  and for a wide range of  $Q^2$  [28]. However, it obviously fails describing the hadronic total cross sections, since it never exceeds the value 23.03 mb. The  $x$ -dependence guarantees Bjorken scaling for DIS at high  $Q^2$ , however, Bjorken  $x$  is not a well defined quantity in the soft limit.

This problem as well as the difficulty with the definition of  $x$  have been fixed in [29], where the dipole cross section is treated as a function of the *c.m.* energy  $\sqrt{s}$ , rather than  $x$ , since  $\sqrt{s}$  is more appropriate for hadronic processes. A similarly simple form for the dipole cross section is used

$$\text{“KST”}: \quad \sigma_{q\bar{q}}(r, s) = \sigma_0(s) \left[ 1 - e^{-r^2/r_0^2(s)} \right] . \quad (14)$$

The values and energy dependence of hadronic cross sections is guaranteed by the choice of

$$\sigma_0(s) = 23.6 \left( \frac{s}{s_0} \right)^{0.08} \left( 1 + \frac{3}{8} \frac{r_0^2(s)}{\langle r_{ch}^2 \rangle} \right) \text{ mb} , \quad (15)$$

$$r_0(s) = 0.88 \left( \frac{s}{s_0} \right)^{-0.14} \text{ fm} . \quad (16)$$

The energy dependent radius  $r_0(s)$  is fitted to data for the proton structure function  $F_2^p(x, Q^2)$ ,  $s_0 = 1000 \text{ GeV}^2$  and the mean square of the pion charge radius  $\langle r_{ch}^2 \rangle = 0.44 \text{ fm}^2$ . The improvement at large separations leads to a somewhat worse description of the proton structure function at large  $Q^2$ . Apparently, the cross section dependent on energy, rather than  $x$ , cannot provide Bjorken scaling. Indeed, the parameterization Eq. (14) is successful only up to  $Q^2 \approx 10 \text{ GeV}^2$ .

In fact, the cases we are interested in, charmonium production and interaction, are just in between the regions where either of these parameterization is successful. Therefore, we suppose that the difference between predictions using Eqs. (13) and (14) is a measure of the theoretical uncertainty which fortunately turns out to be rather small.

We demonstrate in Fig. 2 a few examples of  $r^2$ -dependence of the dipole cross section at different energies for both parameterization. Both, GBW and KST cross section, vanish  $\propto r^2$  at small  $r$ , but deviate considerably from this simple behavior at large separations.

Quite often, the simplest parameterization ( $\propto r^2$ ) is used for the dipole cross section. For the coefficient in front of  $r^2$  we employ the expression obtained by the first term of the Taylor expansion of Eq. (14):

$$\text{“}r^2\text{”}: \quad \sigma_{q\bar{q}}(r, s) = \frac{\sigma_0(s)}{r_0^2(s)} \cdot r^2 . \quad (17)$$

We shall refer to this form of the dipole cross section as  $r^2$ -approximation.

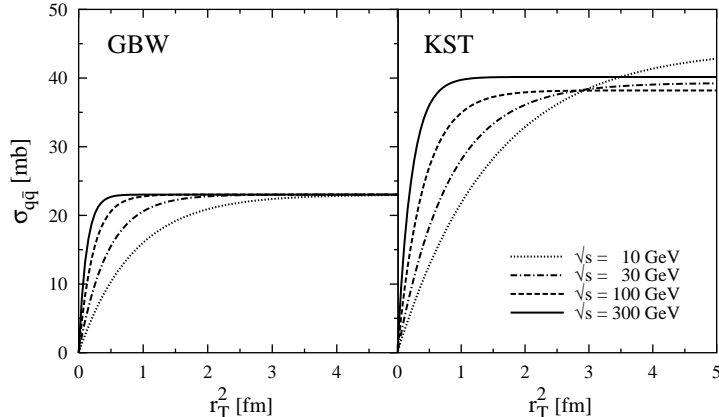


**Fig. 2.** The dipole cross section as function of  $r_T^2$  at energies  $\sqrt{s} = 10, 30, 100$  and  $300$  GeV for GBW (left) and KST (right) parameterizations. In the left panel, we used the prescription of [30],  $x = (M_\psi^2 + Q^2)/s$ , where  $M_\psi$  is the charmonium mass.

#### 4 Diffractive photoproduction of charmonia off protons

The dynamics of production and interaction of charmonia has drawn attention since their discovery back in 1974 [31]. As these heavy mesons have a small size it has been expected that hadronic cross sections may be calculated relying on perturbative QCD. The study of charmonium production became even more intense after charmonium suppression had been suggested as a probe for the creation and interaction of quark-gluon plasma in relativistic heavy ion collisions [12].

Since we will never have direct experimental information on charmonium-nucleon total cross sections one has to extract it from other data for example from elastic photoproduction of charmonia  $\gamma p \rightarrow J/\psi(\psi') p$ . The widespread belief that one can rely on the vector dominance model (VDM) is based on previous experience with photoproduction of  $\rho$  mesons. However, even a dispersion approach shows that this is quite a risky way, because the  $J/\psi$  pole in the complex  $Q^2$  plane is nearly 20 times farther away from the physical region than the  $\rho$  pole. The multichannel analysis performed in [32] demonstrates that the corrections are huge,  $\sigma_{tot}^{J/\psi p}$  turns out to be more than three times larger than the VDM prediction. Unfortunately, more exact predictions of the multichannel approach, especially for  $\psi'$ , need knowledge of many diagonal and off-diagonal amplitudes which are easily summed only if one uses the oversimplified oscillator wave functions and a  $q\bar{q}$ -proton cross section of the form  $\sigma_{q\bar{q}}(r) \propto r^2$ , where  $r$  is the transverse  $q\bar{q}$  separation.

Instead, one may switch to the quark basis, which should be equivalent to the hadronic basis because of completeness. In this representation the procedure of extracting  $\sigma_{tot}^{J/\psi p}$  from photoproduction data cannot be realized directly, but has to be replaced by a different strategy. Namely, as soon as one has expressions for



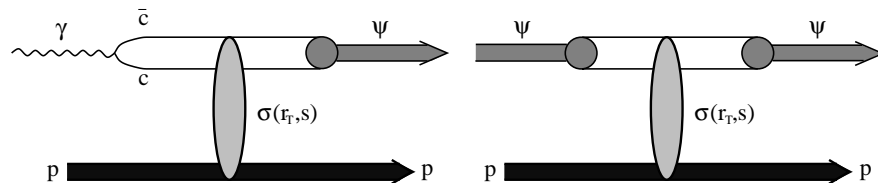


**Fig. 3.** Schematic representation of the amplitudes for the reactions  $\gamma^* p \rightarrow \psi p$  (left) and  $\psi p$  elastic scattering (right) in the rest frame of the proton. The  $c\bar{c}$  fluctuation of the photon and the  $\psi$  with transverse separation  $r$  and c.m. energy  $\sqrt{s}$  interact with the target proton via the cross section  $\sigma(r,s)$  and produce a  $J/\psi$  or  $\psi'$ .

the wave functions of charmonia and the universal dipole cross section  $\sigma_{q\bar{q}}(r,s)$ , one can predict both, the experimentally known charmonium photoproduction cross sections and the unknown  $\sigma_{tot}^{J/\psi(\psi')p}$ . If the photoproduction data are well described one may have some confidence in the predictions for the  $\sigma_{tot}^{J/\psi(\psi')p}$ . Of course this procedure will be model dependent, but we believe that this is the best use of photoproduction data one can presently make. This program was performed for the first time in [33]. We do not propose a conceptually new scheme here, but calculate within a given approach as accurately as possible and without any free parameters. Wherever there is room for arbitrariness, like forms for the color dipole cross section and those for charmonium wave functions, we use and compare other author's proposals, which have been tested on data different from those used here.

In the light-cone dipole approach the two processes, photoproduction and charmonium-nucleon elastic scattering look as shown in Fig. 3 [33]. The corresponding expressions for the forward amplitudes read

$$\mathcal{M}_{\gamma^* p}(s, Q^2) = \sum_{\mu, \bar{\mu}} \int_0^1 d\alpha \int d^2\mathbf{r} \Phi_{\psi}^{*(\mu, \bar{\mu})}(\alpha, \mathbf{r}) \sigma_{q\bar{q}}(r, s) \Phi_{\gamma^*}^{(\mu, \bar{\mu})}(\alpha, \mathbf{r}, Q^2), \quad (18)$$

$$\mathcal{M}_{\psi p}(s) = \sum_{\mu, \bar{\mu}} \int_0^1 d\alpha \int d^2\mathbf{r} \Phi_{\psi}^{*(\mu, \bar{\mu})}(\alpha, \mathbf{r}) \sigma_{q\bar{q}}(r, s) \Phi_{\psi}^{(\mu, \bar{\mu})}(\alpha, \mathbf{r}). \quad (19)$$

Here the summation runs over spin indexes  $\mu, \bar{\mu}$  of the  $c$  and  $\bar{c}$  quarks,  $Q^2$  is the photon virtuality,  $\Phi_{\gamma^*}(\alpha, r, Q^2)$  is the light-cone distribution function of the photon for a  $c\bar{c}$  fluctuation of separation  $r$  and relative fraction  $\alpha$  of the photon light-cone momentum carried by  $c$  or  $\bar{c}$ . Correspondingly,  $\Phi_{\psi}(\alpha, \mathbf{r})$  is the light-cone wave function of  $J/\psi, \psi'$  and  $\chi$  (only in Eq. 19). The dipole cross section  $\sigma_{q\bar{q}}(r, s)$  mediates the transition (*cf* Fig. 3).

The light cone variable describing longitudinal motion which is invariant to Lorentz boosts is the fraction  $\alpha = p_c^+ / p_{\gamma^*}^+$  of the photon light-cone momentum  $p_{\gamma^*}^+ = E_{\gamma^*} + p_{\gamma^*}$  carried by the quark or antiquark. In the nonrelativistic approximation (assuming no relative motion of  $c$  and  $\bar{c}$ )  $\alpha = 1/2$  (e.g. [33]), otherwise one should integrate over  $\alpha$  (see Eq. (18)). For transversely ( $T$ ) and longitudo-

nally ( $L$ ) polarized photons the perturbative photon-quark distribution function in Eq. (18) reads [19,20],

$$\Phi_{T,L}^{(\mu,\bar{\mu})}(\alpha, \mathbf{r}, Q^2) = \frac{\sqrt{N_c} \alpha_{em}}{2\pi} Z_c \chi_c^{\mu\dagger} \widehat{O}_{T,L} \widetilde{\chi}_{\bar{c}}^{\bar{\mu}} K_0(\varepsilon r), \quad (20)$$

where

$$\widetilde{\chi}_{\bar{c}} = i \sigma_y \chi_{\bar{c}}^*; \quad (21)$$

$\chi$  and  $\bar{\chi}$  are the spinors of the  $c$ -quark and antiquark respectively;  $Z_c = 2/3$ .  $K_0(\varepsilon r)$  is the modified Bessel function with

$$\varepsilon^2 = \alpha(1 - \alpha)Q^2 + m_c^2. \quad (22)$$

The operators  $\widehat{O}_{T,L}$  have the form:

$$\widehat{O}_T = m_c \boldsymbol{\sigma} \cdot \mathbf{e}_\gamma + i(1 - 2\alpha) (\boldsymbol{\sigma} \cdot \mathbf{n}) (\mathbf{e}_\gamma \cdot \nabla_r) + (\mathbf{n} \times \mathbf{e}_\gamma) \cdot \nabla_r, \quad (23)$$

$$\widehat{O}_L = 2Q\alpha(1 - \alpha) \boldsymbol{\sigma} \cdot \mathbf{n}, \quad (24)$$

where  $\mathbf{n} = \mathbf{p}/p$  is a unit vector parallel to the photon momentum and  $\mathbf{e}$  is the polarization vector of the photon. Effects of the non-perturbative interaction within the  $q\bar{q}$  fluctuation are negligible for the heavy charmed quarks.

#### 4.1 Charmonium wave functions

The spatial part of the  $c\bar{c}$  pair wave function satisfying the Schrödinger equation

$$\left( -\frac{\Delta}{m_c} + V(R) \right) \Psi_{nlm}(\mathbf{R}) = E_{nl} \Psi_{nlm}(\mathbf{R}) \quad (25)$$

is represented in the form

$$\Psi(\mathbf{R}) = \Psi_{nl}(R) \cdot Y_{lm}(\theta, \varphi), \quad (26)$$

where  $\mathbf{R}$  is 3-dimensional  $c\bar{c}$  separation (not to be confused with the 2-dimensional argument  $\mathbf{r}$  of the dipole cross section),  $\Psi_{nl}(R)$  and  $Y_{lm}(\theta, \varphi)$  are the radial and orbital parts of the wave function. The equation for radial  $\Psi(R)$  is solved with the help of the program [34]. The following four potentials  $V(R)$  have been used:

- “COR”: Cornell potential [35],

$$V(r) = -\frac{k}{R} + \frac{R}{a^2} \quad (27)$$

with  $k = 0.52$ ,  $a = 2.34 \text{ GeV}^{-1}$  and  $m_c = 1.84 \text{ GeV}$ .

- “BT”: Potential suggested by Buchmüller and Tye [36] with  $m_c = 1.48 \text{ GeV}$ . It has a similar structure as the Cornell potential: linear string potential at large separations and Coulomb shape at short distances with some refinements, however.

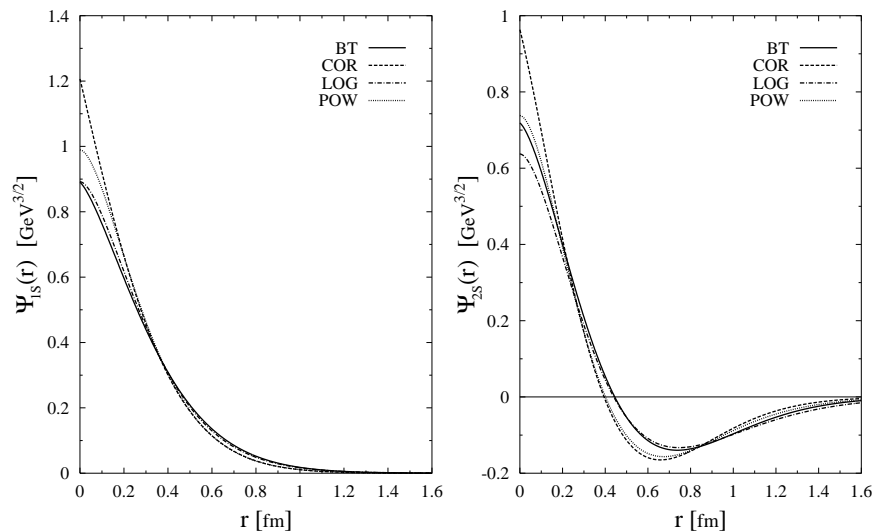


**Fig. 4.** The radial part of the wave function  $\Psi_{nl}(r)$  for the  $1S$  and  $2S$  states calculated with four different potentials (see text). In this figure,  $r = R$ .

- “LOG”: Logarithmic potential [37]

$$V(R) = -0.6635 \text{ GeV} + (0.733 \text{ GeV}) \log(R \cdot 1 \text{ GeV}) \quad (28)$$

with  $m_c = 1.5 \text{ GeV}$ .

- “POW”: Power-law potential [38]

$$V(R) = -8.064 \text{ GeV} + (6.898 \text{ GeV})(R \cdot 1 \text{ GeV})^{0.1} \quad (29)$$

with  $m_c = 1.8 \text{ GeV}$ .

The results of calculations for the radial part  $\Psi_{nl}(R)$  of the  $1S$  and  $2S$  states are depicted in Fig. 4. For the ground state all the potentials provide a very similar behavior for  $R > 0.3 \text{ fm}$ , while for small  $R$  the predictions are differ by up to 30%. The peculiar property of the  $2S$  state wave function is the node at  $R \approx 0.4 \text{ fm}$  which causes strong cancelations in the matrix elements Eq. (18) and as a result, a suppression of photoproduction of  $\psi'$  relative to  $J/\psi$  [33,39].

Note that the lowest Fock component  $|c\bar{c}\rangle$  in the infinite momentum frame is not related by simple Lorentz boost to the wave function of charmonium in the rest frame. This makes the problem of building the light-cone wave function for the lowest  $|c\bar{c}\rangle$  component difficult, no unambiguous solution is yet known. There are only recipes in the literature, a simple one widely used [40], is the following. One applies a Fourier transformation from coordinate to momentum space to the known spatial part of the non-relativistic wave function (26),  $\Psi(\mathbf{R}) \Rightarrow \Psi(\mathbf{p})$ , which can be written as a function of the effective mass of the  $c\bar{c}$ ,  $M^2 = 4(p^2 + m_c^2)$ , expressed in terms of light-cone variables

$$M^2(\alpha, p_T) = \frac{p_T^2 + m_c^2}{\alpha(1-\alpha)}. \quad (30)$$

In order to change the integration variable  $p_L$  to the light-cone variable  $\alpha$  one relates them through  $M$ , namely  $p_L = (\alpha - 1/2)M(p_T, \alpha)$ . In this way the  $c\bar{c}$  wave function acquires a kinematical factor

$$\Psi(\mathbf{p}) \Rightarrow \sqrt{2} \frac{(p^2 + m_c^2)^{3/4}}{(p_T^2 + m_c^2)^{1/2}} \cdot \Psi(\alpha, \mathbf{p}_T) \equiv \Phi_\psi(\alpha, \mathbf{p}_T) . \quad (31)$$

This procedure is used in [41] and the result is applied to calculation of the amplitudes (18). The result is discouraging, since the  $\psi'$  to  $J/\psi$  ratio of the photoproduction cross sections are far too low in comparison with data. However, the oversimplified dipole cross section  $\sigma_{q\bar{q}}(r) \propto r^2$  has been used, and what is even more essential, the important ingredient of Lorentz transformations, the Melosh spin rotation, has been left out. The spin transformation has also been left out in the recent publication [42] which repeats the calculations of [41] with a more realistic dipole cross section which levels off at large separations. This leads to suppression of the node-effect (less cancelation) and enhancement of  $\Psi'$  photoproduction. Nevertheless, the calculated  $\psi'$  to  $J/\psi$  ratio is smaller than the data by a factor of two.

The 2-spinors  $\chi_c$  and  $\chi_{\bar{c}}$  describing  $c$  and  $\bar{c}$  respectively in the infinite momentum frame are known to be related by Melosh rotation [43,40] to the spinors  $\bar{\chi}_c$  and  $\bar{\chi}_{\bar{c}}$  in the rest frame:

$$\begin{aligned} \bar{\chi}_c &= \widehat{R}(\alpha, \mathbf{p}_T) \chi_c , \\ \bar{\chi}_{\bar{c}} &= \widehat{R}(1 - \alpha, -\mathbf{p}_T) \chi_{\bar{c}} , \end{aligned} \quad (32)$$

where the matrix  $\widehat{R}(\alpha, \mathbf{p}_T)$  has the form:

$$\widehat{R}(\alpha, \mathbf{p}_T) = \frac{m_c + \alpha M - i [\boldsymbol{\sigma} \times \mathbf{n}] \cdot \mathbf{p}_T}{\sqrt{(m_c + \alpha M)^2 + p_T^2}} . \quad (33)$$

Since the potentials we use in section 4.1 contain no spin-orbit term, the  $c\bar{c}$  pair is in  $S$ -wave. In this case spatial and spin dependences in the wave function factorize and we arrive at the following light cone wave function of the  $c\bar{c}$  in the infinite momentum frame

$$\Phi_\psi^{(\mu, \bar{\mu})}(\alpha, \mathbf{p}_T) = U^{(\mu, \bar{\mu})}(\alpha, \mathbf{p}_T) \cdot \Phi_\psi(\alpha, \mathbf{p}_T) , \quad (34)$$

where

$$U^{(\mu, \bar{\mu})}(\alpha, \mathbf{p}_T) = \chi_c^{\mu\dagger} \widehat{R}^\dagger(\alpha, \mathbf{p}_T) \boldsymbol{\sigma} \cdot \mathbf{e}_\psi \sigma_y \widehat{R}^*(1 - \alpha, -\mathbf{p}_T) \sigma_y^{-1} \widetilde{\chi}_{\bar{c}}^{\bar{\mu}} \quad (35)$$

and  $\widetilde{\chi}_{\bar{c}}$  is defined in (21).

Note that the wave function (34) is different from one used in [44–46] where it was assumed that the vertex  $\psi \rightarrow c\bar{c}$  has the structure  $\psi_\mu \bar{u} \gamma_\mu u$  like the for the photon  $\gamma^* \rightarrow c\bar{c}$ . The rest frame wave function corresponding to such a vertex contains  $S$  wave and  $D$  wave. The weight of the latter is dictated by the structure of the vertex and cannot be justified by any reasonable nonrelativistic potential model for the  $c\bar{c}$  interaction.

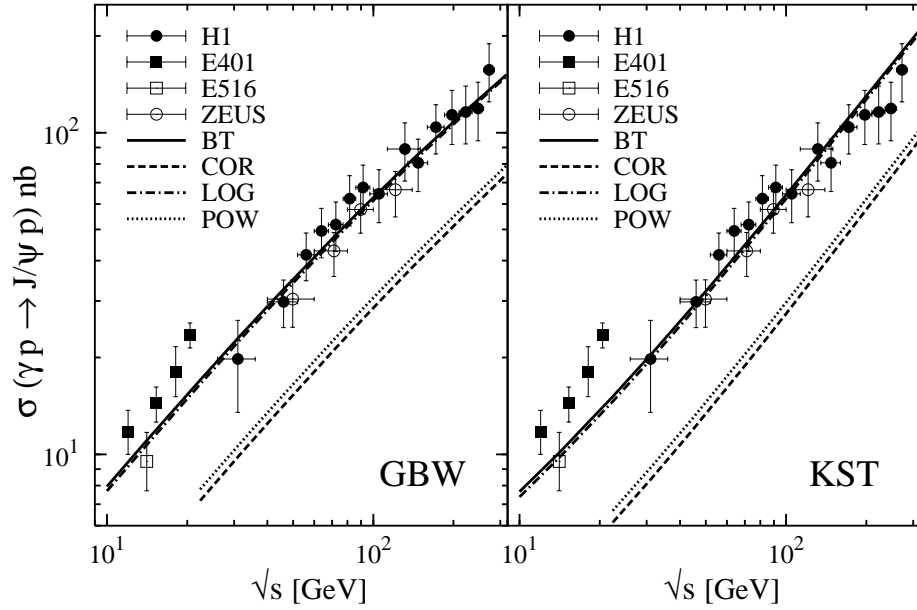


**Fig. 5.** Integrated cross section for elastic photoproduction  $\gamma p \rightarrow J/\psi p$  with real photons ( $Q^2 = 0$ ) as a function of the energy calculated with GBW and KST dipole cross sections and for four potentials to generate  $J/\psi$  wave functions. Experimental data points from the H1 [47], E401 [48], E516 [49] and ZEUS [50] experiments.

Now we can determine the light-cone wave function in the mixed longitudinal momentum - transverse coordinate representation:

$$\Phi_{\psi}^{(\mu, \bar{\mu})}(\alpha, \mathbf{r}) = \frac{1}{2\pi} \int d^2 \mathbf{p}_T e^{-i \mathbf{p}_T \mathbf{r}} \Phi_{\psi}^{(\mu, \bar{\mu})}(\alpha, \mathbf{p}_T). \quad (36)$$

## 4.2 Comparison with data

Having the light-cone wave function of charmonium, we are now in the position to calculate the cross section of charmonium photoproduction using Eq. (18). The results for  $J/\psi$  are compared with the data in Fig. 5. Calculations are performed with GBW and KST parameterizations for the dipole cross section and for wave functions of the  $J/\psi$  calculated from BT, LOG, COR and POW potentials. One observes

- There are no major differences between different parameterizations [28,29] of the dipole cross section.
- The use of different potentials to generate the wave functions of the  $J/\psi$  leads to two distinctly different behaviors. The potentials labeled BT and LOG (see sect. 4.1) describe the data very well, while the potentials COR and LOG underestimate them by a factor of two. The different behavior has been traced to the following origin: BT and LOG use  $m_c \approx 1.5$  GeV, but

		BT	LOG	COR	POW
$\sigma$	GBW	52.01 (37.77)	50.78 (36.63)	23.13 (17.07)	24.94 (18.64)
	KST	49.96 (35.87)	48.49 (34.57)	21.05 (15.42)	22.83 (16.92)
	$r^2$	66.67 (47.00)	64.07 (44.86)	25.81 (18.71)	28.23 (20.66)
$\mathcal{R}$	GBW	0.147 (0.075)	0.117 (0.060)	0.168 (0.099)	0.144 (0.085)
	KST	0.147 (0.068)	0.118 (0.054)	0.178 (0.099)	0.152 (0.084)
	$r^2$	0.101 (0.034)	0.081 (0.027)	0.144 (0.070)	0.121 (0.058)

**Table 1.** The photoproduction  $\gamma p \rightarrow J/\psi p$  cross-section  $\sigma(J/\psi)$  in nb and the ratio  $\mathcal{R} = \sigma(\psi')/\sigma(J/\psi)$  for the four different types of potentials (BT, LOG, COR, POW) and the three parameterizations (GBW, KST,  $r^2$ ) for the dipole cross section  $\sigma(r, s)$  at  $\sqrt{s} = 90$  GeV. The values in parentheses correspond to the case when the spin rotation is neglected. See Ref. [1] for a comparison with data.

COR and POW  $m_c \approx 1.8$  GeV. While the bound state wave functions of  $J/\psi$  are little affected by this difference (see Fig. 4), the photon wave function Eq. (20) depends sensitively on  $m_c$  via the argument Eq. (22) of the  $K_0$  function.

### 4.3 Importance of spin effects for the $\psi'$ to $J/\psi$ ratio

It turns out that the effects of spin rotation have a gross impact on the cross section of elastic photoproduction  $\gamma p \rightarrow J/\psi(\psi')p$ . To demonstrate these effects we present the results of our calculations at  $\sqrt{s} = 90$  GeV in Table 1. The upper half of the table shows the photoproduction cross sections for  $J/\psi$  for different parameterizations of the dipole cross section (GBW, KST, “ $r^2$ ”) and potentials (BT, COR, LOG, POW). The numbers in parenthesis show what the cross section would be, if the spin rotation effects were neglected. We see that these effects add 30-40% to the  $J/\psi$  photoproduction cross section.

The spin rotation effects turn out to have a much more dramatic impact on  $\psi'$  increasing the photoproduction cross section by a factor 2-3. This is visible in the lower half of the table which shows the ratio  $\mathcal{R} = \sigma(\psi')/\sigma(J/\psi)$  of photoproduction cross sections, where the number in parenthesis correspond to no spin rotation effects included. This spin effects explain the large values of the ratio  $\mathcal{R}$  observed experimentally. Our results for  $\mathcal{R}$  are about twice as large as evaluated in [42] and even more than in [41].

### 4.4 Charmonium-nucleon total cross sections

After the light-cone formalism has been checked with the data for virtual photoproduction we are in position to provide reliable predictions for charmonium-nucleon total cross sections. The corresponding expressions are given by Eq. (19))

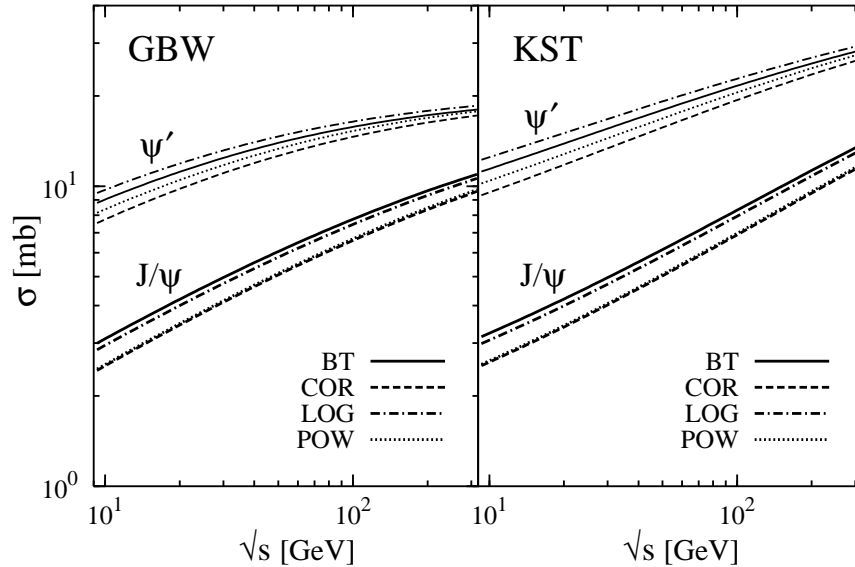


**Fig. 6.** Total  $J/\psi p$  (thick curves) and  $\psi' p$  (thin curves) cross sections with the GBW and KST parameterizations for the dipole cross section.

(compare with [13]). The calculated  $J/\psi$ - and  $\psi'$ -nucleon total cross sections are plotted in Fig. 6 for for the GBW and KST forms of the dipole cross sections and all four types of the charmonium potentials.

## 5 Nuclear effects in exclusive leptonproduction of charmonia

Charmonium production on nuclei can be exclusive,  $\gamma^* A \rightarrow \Psi X$ , where  $X = A$  (coherent) or  $X = A^*$  (incoherent), and inclusive when  $X$  includes pions. We skip the latter which is discussed in [51] and concentrate here on exclusive processes. In this case the following phenomena are to be expected: color filtering, *i.e.* inelastic interactions of the  $c\bar{c}$  pair on its way through the nucleus is expected to lead to a suppression of  $\Psi$  production relative to  $A\sigma_{\gamma^* p \rightarrow \Psi p}$ . Since the dipole cross section  $\sigma_{q\bar{q}}$  also depends on the gluon distribution in the target ( $p$  of  $A$ ), nuclear shadowing of the gluon distribution is expected to reduce  $\sigma_{q\bar{q}}$  in a nuclear reaction relative to the one on the proton. Production of a  $c\bar{c}$  pair in a nucleus and its absorption are also determined by the values of the coherence length  $l_c$  and the formation length  $l_f$  [23].

Explicit calculations have been performed in Ref. [33] in the approximation of a short coherence (or production) length, when one can treat the creation of the colorless  $c\bar{c}$  pair as instantaneous,

$$l_c = \frac{2\nu}{M_{c\bar{c}}^2} \approx \frac{2\nu}{M_{J/\psi}^2} \ll R_A, \quad (37)$$

where  $\nu$  is the energy of the virtual photon in the rest frame of the nucleus. At the same time, the formation length may be long, comparable with the nuclear radius  $R_A$ ,

$$l_f = \frac{2\nu}{M_{\psi'}^2 - M_{J/\psi}^2} \sim R_A . \quad (38)$$

In Ref. [33] the wave function formation is described by means of the light-cone Green function approach summing up all possible paths of the  $c\bar{c}$  in the nucleus. The result has been unexpected. Contrary to naive expectation, based on the larger size of the  $\psi'$  compared to  $J/\psi$ , it has been found that  $\psi'$  is not more strongly absorbed than the  $J/\psi$ , but may even be enhanced by the nuclear medium. This is interpreted as an effect of filtering which is easy to understand in the limit of long coherence length,  $l_c \gg R_A$ . Indeed, the production rate of  $\psi'$  on a proton target is small due to strong cancellations in the projection of the produced  $c\bar{c}$  wave packet onto the radial wave function of the  $\psi'$  which has a node. After propagation through nuclear matter the transverse size of a  $c\bar{c}$  wave packet is squeezed by absorption and the projection of the  $\psi'$  wave function is enhanced [33,39] since the effect of the node is reduced (see another manifestation of the node in [52]).

However, the quantitative predictions of [33] are not trustable since the calculations have been oversimplified and quite some progress has been made on the form of the dipole cross section  $\sigma_{q\bar{q}}$  and the light cone wave functions for the charmonia. Therefore we take the problem up again and provide more realistic calculations for nuclear effects in exclusive electroproduction of charmonia off nuclei relying on the successful parameter free calculations which have been performed recently in Ref. [1] for elastic virtual photoproduction of charmonia,  $\gamma^* p \rightarrow \Psi p$  (see sect. 4).

Whenever one deals with high-energy reactions on nuclei, one cannot avoid another problem of great importance: gluon shadowing. At small values of  $x$ , gluon clouds overlap in longitudinal direction and may fuse. As a result, the gluon density per one nucleon in a nucleus is expected to be reduced compared to a free proton. Parton shadowing, which leads to an additional nuclear suppression in various hard reactions (DIS, DY, heavy flavor, high- $p_T$  hadrons, etc.) may be especially strong for exclusive vector meson production like charmonium production which needs at least two gluon exchange. Unfortunately, we have no experimental information for gluon shadowing in nuclei so far, and we have to rely on the available theoretical estimates, see *e.g.* Refs. [53,18,29,54].

### 5.1 Eikonal shadowing versus absorption for $c\bar{c}$ pairs in nuclei

Exclusive charmonium production off nuclei,  $\gamma^* A \rightarrow \Psi X$  is called coherent, when the nucleus remains intact, i.e.  $X = A$ , or incoherent, when  $X$  is an excited nuclear state which contains nucleons and nuclear fragments but no other hadrons. The cross sections depend on the polarization  $\epsilon$  of the virtual photon (in all figures below we will imply  $\epsilon = 1$ ),

$$\sigma^{\gamma^* A}(s, Q^2) = \sigma^{\gamma_T^* A}(s, Q^2) + \epsilon \sigma^{\gamma_L^* A}(s, Q^2) , \quad (39)$$



where the indexes  $T, L$  correspond to transversely or longitudinally polarized photons, respectively.

The cross section for exclusive production of charmonia off a nucleon target integrated over momentum transfer [13] is given by

$$\sigma_{inc}^{\gamma_{T,L}^* N}(s, Q^2) = \left| \left\langle \Psi \left| \sigma_{q\bar{q}}(r, s) \right| \gamma_{c\bar{c}}^{T,L} \right\rangle \right|^2, \quad (40)$$

where  $\Psi(\mathbf{r}, \alpha)$  is the charmonium LC wave function which depends on the transverse  $c\bar{c}$  separation  $\mathbf{r}$  and on the relative sharing  $\alpha$  of longitudinal momentum [1]. Both variables are involved in the integration in the matrix element Eq. (40).  $\Psi(\mathbf{r}, \alpha)$  is obtained by means of a Lorentz boost applied the solutions of the Schrödinger equation. This procedure involves the Melosh spin rotation [40,43] which produces sizable effects. In addition,  $\gamma_{c\bar{c}}^{T,L}(\mathbf{r}, \alpha, Q^2)$  is the LC wave function of the  $c\bar{c}$  Fock component of the photon. It depends on the photon virtuality  $Q^2$ . One can find the details in Ref. [1] including the effects of a nonperturbative  $q\bar{q}$  interaction.

The cross sections for coherent and incoherent production on nuclei will be derived under various conditions imposed by the coherence length Eq. (37). At high energies the coherence length Eq. (37) may substantially exceed the nuclear radius. In this case the transverse size of the  $c\bar{c}$  wave packet is “frozen” by Lorentz time dilation, *i.e.* it does not fluctuate during propagation through the nucleus, and the expressions for the cross sections, incoherent (*inc*) or coherent (*coh*), are particularly simple [33],

$$\sigma_{inc}^{\gamma_{T,L}^* A}(s, Q^2) = \int d^2b T_A(b) \left| \left\langle \Psi \left| \sigma_{q\bar{q}}(r, s) \exp \left[ -\frac{1}{2} \sigma_{q\bar{q}}(r, s) T_A(b) \right] \right| \gamma_{c\bar{c}}^{T,L} \right\rangle \right|^2 \quad (41)$$

$$\sigma_{coh}^{\gamma_{T,L}^* A}(s, Q^2) = \int d^2b \left| \left\langle \Psi \left| 1 - \exp \left[ -\frac{1}{2} \sigma_{q\bar{q}}(r, s) T_A(b) \right] \right| \gamma_{c\bar{c}}^{T,L} \right\rangle \right|^2. \quad (42)$$

Here  $T_A(b) = \int_{-\infty}^{\infty} dz \rho_A(b, z)$  is the nuclear thickness function given by the integral of the nuclear density along the trajectory at a given impact parameter  $b$ .

The nuclear suppression ratio for incoherent electroproduction of  $J/\psi$  and  $\psi'$  is shown in Fig. 7 as a function of  $\sqrt{s}$ . We use the GBW [28] and KST [29] parameterizations for the dipole cross section and show the results by solid and dashed curves, respectively. Differences are at most 10 – 20%. Analyzing the results shown in Fig. 7, we observe that nuclear suppression of  $J/\psi$  production becomes stronger with energy. This is an obvious consequence of the energy dependence of  $\sigma_{q\bar{q}}(r, s)$ , which rises with energy (see sect. 3). For  $\psi'$  the suppression is rather similar to the  $J/\psi$  case. In particular we do not see any considerable nuclear enhancement of  $\psi'$  which has been found earlier [33,55], where the oversimplified form of the dipole cross section,  $\sigma_{q\bar{q}}(r) \propto r^2$  and the oscillator form of the wave function had been used. Such a form of the cross section enhances the compensation between large and small distances in the wave function of  $\psi'$  in the process  $\gamma^* p \rightarrow \psi' p$ . Therefore, the color filtering effect which emphasizes

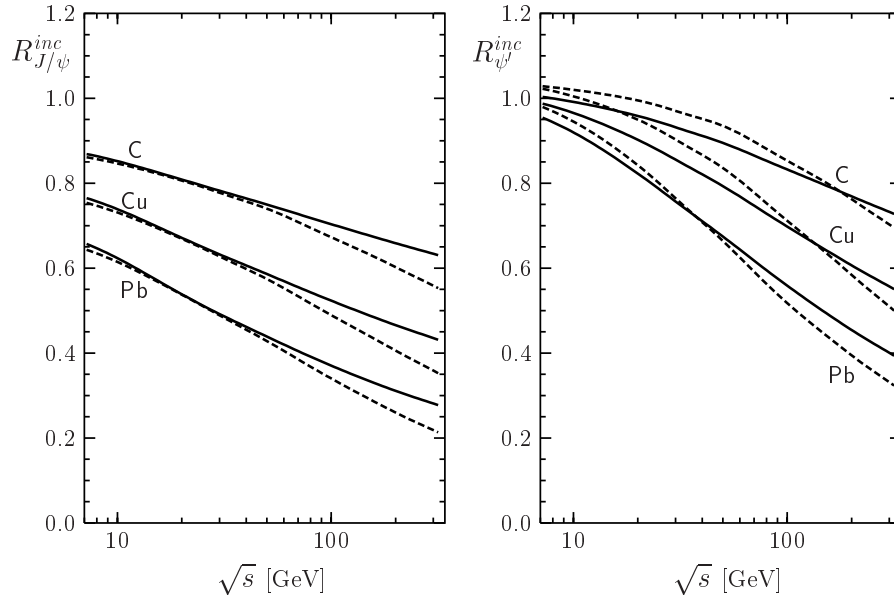


**Fig. 7.** Ratios  $R_{\psi'}^{inc}$  for  $J/\psi$  and  $\psi'$  incoherent production on carbon, copper and lead as function of  $\sqrt{s}$  and at  $Q^2 = 0$ . The solid curves refer to the GBW parameterization of  $\sigma_{q\bar{q}}$  and dashed one refer to the KST parameterization.

the small distance part of the wave function leads to a strong enhancement of the  $\psi'$  production rate. This is why using the more realistic  $r$ -dependence of  $\sigma_{q\bar{q}}(r)$  leveling off at large  $r$  leads to a weaker enhancement of the  $\psi'$ . This effect becomes even more pronounced at higher energies since the dipole cross section saturates starting at a value  $r \sim r_0(s)$  where  $r_0(s)$  decreases with energy. This observation probably explains why the  $\psi'$  is less enhanced at higher energies as one can see from Fig. 7.

Note that the “frozen” approximation is valid only for  $l_c \gg R_A$  and can be used only at  $\sqrt{s} > 20 - 30$  GeV. Therefore, the low-energy part of the curves depicted in Fig. 7 should be corrected for the effects related to the finiteness of  $l_c$ . This is done in Ref. [1].

One can change the effect of color filtering in nuclei in a controlled way by increasing the photon virtuality  $Q^2$  thereby squeezing the transverse size of the  $c\bar{c}$  fluctuation in the photon. For a narrower  $c\bar{c}$  pair the cancelation which is caused by the node in the radial wave function of  $\psi'$  should be less effective. One expects that the  $\psi'$  to  $J/\psi$  ratio on a proton target increases with  $Q^2$ , as is observed both in experiment and calculation (Fig. 9 of [1]). A detailed investigation of the  $Q^2$  dependence of nuclear effects is published in Ref. [3].

Cross sections for coherent production of charmonia on nuclei are calculated analogously using Eq. (42). The results for the energy dependence are depicted in Fig. 8.

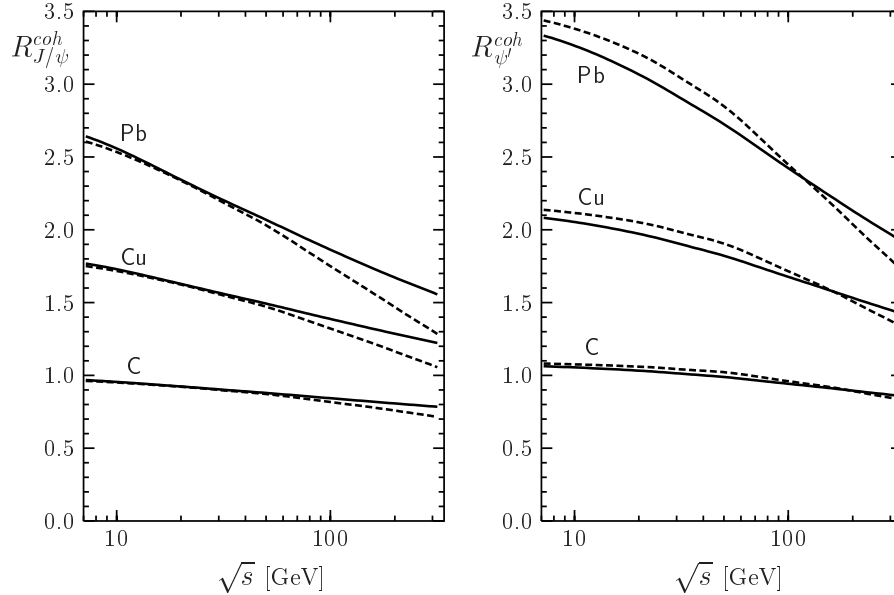


**Fig. 8.** The ratios  $R_{J/\psi}^{coh}$  and  $R_{\psi'}^{coh}$  for coherent production on nuclei as a function of  $\sqrt{s}$ . The meaning of the different lines is the same as in Fig. 7.

It is not a surprise that the ratios exceed one. In the absence of  $c\bar{c}$  attenuation the forward coherent production would be proportional to  $A^2$ , while integrated over momentum transfer, the one depicted in Fig. 8, behaves as  $A^{4/3}$ . This is a result of our definition that  $R_{\psi}^{coh}$  exceeds one.

## 5.2 Gluon shadowing

The gluon density in nuclei at small Bjorken  $x$  is expected to be suppressed compared to a free nucleon due to interferences. This phenomenon called gluon shadowing renormalizes the dipole cross section,

$$\sigma_{q\bar{q}}(r, x) \Rightarrow \sigma_{q\bar{q}}(r, x) R_G(x, Q^2, b). \quad (43)$$

where the factor  $R_G(x, Q^2, b)$  is the ratio of the gluon density at  $x$  and  $Q^2$  in a nucleon of a nucleus to the gluon density in a free nucleon. No data are available so far which could provide direct information about gluon shadowing. Currently it can be evaluated only theoretically. In what follows we employ the technique developed in Ref. [29].

Note that the procedure Eq. (43) differs from the prescription in Ref. [45]. The latter is based on QCD factorization applied to a nuclear target and suggests to multiply by  $R_G(x, Q^2, b)$  the whole nuclear cross section. This approximation should not be used for charmonium production which exposes according to above calculations a strong deviation from factorization. Besides, gluon shadowing is overestimated in Ref. [45] as is discussed in Ref. [29].

The interpretation of the phenomenon of gluon shadowing depends very much on the reference frame. It looks like glue-gluon fusion in the infinite momentum frame of the nucleus: although the nucleus is Lorentz contracted, the bound nucleons are still well separated since they contract too. However, the gluon clouds of the nucleons are contracted less since they have a smaller momentum fraction  $\sim x$ . Therefore, they do overlap and interact at small  $x$ , and gluons originating from different nucleons can fuse leading to a reduction of the gluon density.

Although observables must be Lorentz invariant, the space-time interpretation of shadowing looks very different in the rest frame of the nucleus. Here it comes as a result of eikonalization of higher Fock components of the incident particles. Indeed, the nuclear effect included by eikonalization into Eqs. (41)-(42) corresponds to the lowest  $c\bar{c}$  Fock component of the photon. These expressions do not include any correction for gluon shadowing, but rather correspond to shadowing of sea quarks in nuclei, analogous to what is measured in deep-inelastic scattering. Although the phenomenological dipole cross section  $\sigma_{q\bar{q}}(x, Q^2)$  includes all possible effects of gluon radiation, the eikonal expressions Eqs. (41)-(42) assume that none of the radiated gluons takes part in multiple interaction in the nucleus. The leading order correction corresponding to gluon shadowing comes from eikonalization of the next Fock component which contains the  $c\bar{c}$  pair plus a gluon. One can trace on Feynman graphs that this is exactly the same mechanism of gluon shadowing as glue-gluon fusion in a different reference frame.

Note that Eqs. (41)-(42) assume that for the coherence length  $l_c \gg R_A$ . Even if this condition is satisfied for a  $c\bar{c}$  fluctuation, it can be broken for the  $c\bar{c}G$  component which is heavier. Indeed, it was found in [58] that the coherence length for gluon shadowing is about an order of magnitude shorter than the one for shadowing of sea quarks. Therefore, one should not rely on the long coherence length approximation used in Eqs. (41)-(42), but take into account the finiteness of  $l_c^G$ . This can be done by using the light-cone Green function approach developed in [56,29].

The factor  $R_G(x, Q^2, b)$  has the form,

$$R_G(x, Q^2, b) = 1 - \frac{\Delta\sigma(\gamma^*A)}{T(b)\sigma(\gamma^*N)}, \quad (44)$$

where  $\sigma(\gamma^*N)$  is the part of the total  $\gamma^*N$  cross section related to a  $c\bar{c}$  fluctuation in the photon,

$$\sigma(\gamma^*N) = \int d^2r \int_0^1 d\alpha |\Psi_{\gamma^* \rightarrow c\bar{c}}(r, \alpha, Q^2)|^2 \sigma_{q\bar{q}}(r, x). \quad (45)$$

Here  $\Psi_{\gamma^* \rightarrow c\bar{c}}(r, \alpha, Q^2)$  is the light-cone wave function of the  $c\bar{c}$  pair with transverse separation  $\mathbf{r}$  and relative sharing of the longitudinal momentum  $\alpha$  and

$1 - \alpha$  (see details in sect. 2). The numerator  $\Delta\sigma(\gamma^* A)$  in (44) reads [29],

$$\begin{aligned} \Delta\sigma(\gamma^* A) &= 8\pi \operatorname{Re} \int dM^2 \left. \frac{d^2\sigma(\gamma^* N \rightarrow c\bar{c}GN)}{dM^2 dq_T^2} \right|_{q_T=0} \\ &\times \int_{-\infty}^{\infty} dz_1 \int_{-\infty}^{\infty} dz_2 \Theta(z_2 - z_1) \rho_A(b, z_1) \rho_A(b, z_2) \exp[-iq_L(z_2 - z_1)] . \end{aligned} \quad (46)$$

Here the invariant mass squared of the  $c\bar{c}G$  system is given by,

$$M^2 = \sum_i \frac{m_i^2 + k_i^2}{\alpha_i} , \quad (47)$$

where the sum is taken over partons ( $c\bar{c}G$ ) having mass  $m_i$ , transverse momentum  $\mathbf{k}_i$  and fraction  $\alpha_i$  of the full momentum. The  $c\bar{c}G$  system is produced diffractively as an intermediate state in a double interaction in the nucleus.  $z_1$  and  $z_2$  are the longitudinal coordinates of the nucleons  $N_1$  and  $N_2$ , respectively, participating in the diffractive transition  $\gamma^* N_1 \rightarrow c\bar{c}G N_1$  and back  $c\bar{c}G N_2 \rightarrow \gamma^* N_2$ . The value of  $\Delta\sigma$  is controlled by the longitudinal momentum transfer

$$q_L = \frac{Q^2 + M^2}{2\nu} , \quad (48)$$

which is related to the gluonic coherence length  $l_c^G = 1/q_L$ .

The Green function  $G_{c\bar{c}G}(\mathbf{r}_2, \boldsymbol{\rho}_2, z_2; \mathbf{r}_1, \boldsymbol{\rho}_1, z_1)$  describes the propagation and interaction of the  $c\bar{c}G$  system in the nuclear medium between the points  $z_1$  and  $z_2$ . Here,  $\mathbf{r}_{1,2}$  and  $\boldsymbol{\rho}_{1,2}$  are the transverse separations between the  $c$  and  $\bar{c}$  and between the  $c\bar{c}$  pair and gluon at the point  $z_1$  and destination  $z_2$  respectively. Then the Fourier transform of the diffractive cross section in Eq. (46),

$$8\pi \int dM_X^2 \left. \frac{d^2\sigma(\gamma^* N \rightarrow XN)}{dM_X^2 dq_T^2} \right|_{q_T=0} \cos[q_L(z_2 - z_1)] \quad (49)$$

can be represented in the form,

$$\begin{aligned} &\frac{1}{2} \operatorname{Re} \int d^2r_2 d^2\rho_2 d^2r_1 d^2\rho_1 \int d\alpha_q d\ln(\alpha_G) \\ &\times F_{\gamma^* \rightarrow c\bar{c}G}^\dagger(\mathbf{r}_2, \boldsymbol{\rho}_2, \alpha_q, \alpha_G) G_{c\bar{c}G}(\mathbf{r}_2, \boldsymbol{\rho}_2, z_2; \mathbf{r}_1, \boldsymbol{\rho}_1, z_1) F_{\gamma^* \rightarrow c\bar{c}G}(\mathbf{r}_1, \boldsymbol{\rho}_1, \alpha_q, \alpha_G) . \end{aligned} \quad (50)$$

Assuming that the momentum fraction taken by the gluon is small,  $\alpha_G \ll 1$ , and neglecting the  $c\bar{c}$  separation  $r \ll \rho$  we arrive at a factorized form of the three-body Green function,

$$G_{c\bar{c}G}(\mathbf{r}_2, \boldsymbol{\rho}_2, z_2; \mathbf{r}_1, \boldsymbol{\rho}_1, z_1) \Rightarrow G_{c\bar{c}}(\mathbf{r}_2, z_2; \mathbf{r}_1, z_1) G_{GG}(\boldsymbol{\rho}_2, z_2; \boldsymbol{\rho}_1, z_1) , \quad (51)$$

where  $G_{GG}(\boldsymbol{\rho}_2, z_2; \boldsymbol{\rho}_1, z_1)$  describes propagation of the  $GG$  dipole (in fact the color-octet  $c\bar{c}$  and gluon) in the nuclear medium. This Green function satisfies

the two dimensional Schrödinger equation which includes the glue-gluon nonperturbative interaction via the light-cone potential  $V(\boldsymbol{\rho}, z)$ , as well as interaction with the nuclear medium.

$$i \frac{d}{dz_2} G_{GG}(\boldsymbol{\rho}_2, z_2; \boldsymbol{\rho}_1, z_1) = \left[ -\frac{\Delta(\boldsymbol{\rho}_2)}{2\nu\alpha_G(1-\alpha_G)} + V(\boldsymbol{\rho}_2, z_2) \right] G_{GG}(\boldsymbol{\rho}_2, z_2; \boldsymbol{\rho}_1, z_1), \quad (52)$$

where

$$2 \operatorname{Im} V(\boldsymbol{\rho}, z) = -\sigma_{GG}(\boldsymbol{\rho}) \rho_A(b, z), \quad (53)$$

and the glue-gluon dipole cross section is related to the  $q\bar{q}$  one by the relation,

$$\sigma_{GG}(r, x) = \frac{9}{4} \sigma_{q\bar{q}}(r, x). \quad (54)$$

Following [29] we assume that the real part of the potential has a form

$$\operatorname{Re} V(\boldsymbol{\rho}, z) = \frac{b_0^4 \rho^2}{2\nu\alpha_G(1-\alpha_G)}. \quad (55)$$

The parameter  $b_0 = 0.65 \text{ GeV}$  was fixed by the data on diffractive gluon radiation (the triple-Pomeron contribution in terms of Regge approach) which is an essential part of Gribov's inelastic shadowing [57]. The well known smallness of such a diffractive cross section explains why  $b_0$  is so large, leading to a rather weak gluon shadowing. In other words, this strong interaction squeezes the glue-gluon wave packet resulting in small nuclear attenuation due to color transparency.

Fig. 9 shows the ratios of cross sections calculated with and without gluon shadowing for incoherent and coherent exclusive charmonium electroproduction. We see that the onset of gluon shadowing happens at a *c.m.* energy of few tens GeV. This onset is controlled by the longitudinal nuclear formfactor

$$F_A(q_c^G, b) = \frac{1}{T_A(b)} \int_{-\infty}^{\infty} dz \rho_A(b, z) e^{iq_c z} \quad (56)$$

where the longitudinal momentum transfer  $q_c^G = 1/l_c^G$ . For the onset of gluon shadowing  $q_c^G R_A \gg 1$  one can keep only the double scattering shadowing correction,

$$S_G \approx 1 - \frac{1}{4} \sigma_{eff} \int d^2b T_A^2(b) F_A^2(q_c^G, b), \quad (57)$$

where  $\sigma_{eff}$  is the effective cross section which depends on the dynamics of interaction of the  $q\bar{q}G$  fluctuation with a nucleon.

It was found in Ref. [58] that the coherence length for gluon shadowing is rather short,

$$l_c^G \approx \frac{1}{10 x m_N}, \quad (58)$$

where  $x$  in our case should be an effective one,  $x = (Q^2 + M_\psi^2)/2m_N\nu$ . The onset of shadowing according to Eqs. (56) and (57) should be expected at  $q_c^2 \sim$

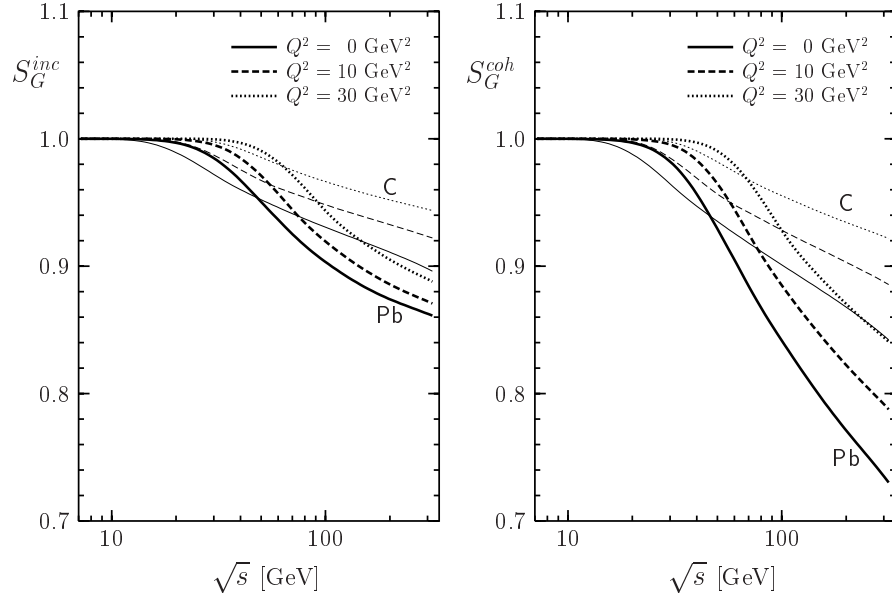


**Fig. 9.** Ratios  $S_G(s, Q^2)$  of cross sections calculated with and without gluon shadowing for incoherent and coherent charmonia production. We only plot ratios for  $J/\psi$  production, because ratios for  $\psi'$  production are practically the same. All curves are calculated with the GBW parameterization of the dipole cross section  $\sigma_{q\bar{q}}$ .

$3/(R_A^{ch})^2$  corresponding to

$$s_G \sim 10m_N R_A^{ch}(Q^2 + M_\psi^2)/\sqrt{3}, \quad (59)$$

where  $(R_A^{ch})^2$  is the mean square of the nuclear charge radius. This estimate is in a good agreement with Fig. 9. Remarkably, the onset of shadowing is delayed with rising nuclear radius and  $Q^2$ . This follows directly from Eq. (57) and the fact that the formfactor is a steeper falling function of  $R_A$  for heavy than for light nuclei, provided that  $q_c^G R_A \gg 1$ .

## 6 Hadroproduction of heavy quarks

We now turn to open heavy flavor production in  $pp$  collisions [4,5]. The color dipole formulation of this process was first introduced in Ref. [59]. In the target rest frame, in which the dipole approach is formulated, heavy quark production looks like pair creation in the target color field, Fig. 10. For a short time, a gluon  $G$  from the projectile hadron can develop a fluctuation which contains a heavy quark pair ( $Q\bar{Q}$ ). Interaction with the color field of the target then may release these heavy quarks. Apparently, the mechanism depicted in Fig. 10 corresponds to the gluon-gluon fusion mechanism of heavy quark production in the leading order (LO) parton model. This can be verified by explicit an

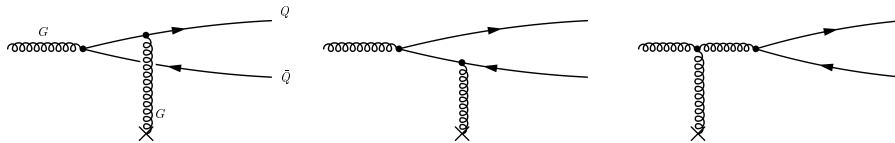


**Fig. 10.** *The three lowest order graphs contributing to heavy quark production in the dipole approach. These graphs correspond to the gluon-gluon fusion mechanism of heavy quark production in the parton model.*

calculation [5]. The dipole formulation is therefore applicable only at low  $x_2$ , where the gluon density of the target is much larger than all quark densities<sup>1</sup>. The kinematical range where the dipole approach is valid can of course only be determined a posteriori. This is similar to determining the minimal value of  $Q^2$  for which perturbative QCD still works. Note that while the mechanism for hadroproduction of heavy quark boundstates is still subject to active theoretical and experimental investigation, the mechanism for open heavy quark production is well established by now [60–62].

We shall now express the process depicted in Fig. 10 in terms of the cross section  $\sigma_{q\bar{q}}(r)$  for scattering a color neutral  $q\bar{q}$ -pair with transverse size  $r$  off a nucleon. The  $Q\bar{Q}$  pair can be produced in three different color and spin states. These states are orthogonal and do not interfere in the cross section. They include:

1. The color-singlet  $C$ -even  $Q\bar{Q}$  state. The corresponding amplitude is odd (O) relative to simultaneous permutation of spatial and spin variables of the  $Q\bar{Q}$  and has the form,

$$A_{ij,a}^{\bar{\mu}\mu}(\boldsymbol{\kappa}, \mathbf{k}_T, \alpha) = \sum_{e=1}^8 \frac{1}{6} \delta_{ae} \delta_{ij} O_e^{\bar{\mu}\mu}(\boldsymbol{\kappa}, \mathbf{k}_T, \alpha) . \quad (60)$$

Here  $\boldsymbol{\kappa}$  and  $\mathbf{k}_T$  are the relative and total transverse momenta of the  $Q\bar{Q}$  pair respectively;  $\mu, \bar{\mu}$  are spin indexes,  $a$  and  $i, j$  are color indexes of the gluon and produced quarks, respectively. We will classify such a state as  $1^-$ , which means a color singlet with odd parity relative to index permutation. Note the  $1^+$  cannot be produced in the reaction shown in Fig. 10 .

2. Color-octet  $Q\bar{Q}$  state with the production amplitude also antisymmetric relative simultaneous permutation of spatial and spin variables of the  $Q\bar{Q}$  ( $8^-$ ),

$$B_{ij,a}^{\bar{\mu}\mu}(\boldsymbol{\kappa}, \mathbf{k}_T, \alpha) = \sum_{e,g=1}^8 \frac{1}{2} d_{aeg} \tau_g(ij) O_e^{\bar{\mu}\mu}(\boldsymbol{\kappa}, \mathbf{k}_T, \alpha) . \quad (61)$$

Here  $\lambda_g = \tau_g/2$  are the Gell-Mann matrices.

<sup>1</sup> We use standard kinematical variables,  $x_2 = 2P_{Q\bar{Q}} \cdot P_1/s$  and  $x_1 = 2P_{Q\bar{Q}} \cdot P_2/s$ , where  $P_1$  ( $P_2$ ) is the four-momentum of the projectile (target) hadron, and  $P_{Q\bar{Q}}$  is the four-momentum of the heavy quark pair. In addition,  $M_{Q\bar{Q}}$  is the invariant mass of the pair, and  $s$  is the hadronic center of mass energy squared.



3. Color-octet  $Q\bar{Q}$  with the amplitude symmetric relative permutation of quark variables ( $8^+$ ),

$$C_{ij,a}^{\bar{\mu}\mu}(\boldsymbol{\kappa}, \mathbf{k}_T, \alpha) = \sum_{e,g=1}^8 \frac{i}{2} f_{aeg} \tau_g(ij) E_e^{\bar{\mu}\mu}(\boldsymbol{\kappa}, \mathbf{k}_T, \alpha) . \quad (62)$$

The two amplitudes in Eq. (60) and (61) contain the common factor

$$O_e^{\bar{\mu}\mu}(\boldsymbol{\kappa}, \mathbf{k}_T, \alpha) = \int d^2r d^2s e^{i\boldsymbol{\kappa}\cdot\mathbf{r}-i\mathbf{k}_T\cdot\mathbf{s}} \Psi_{Q\bar{Q}}^{\bar{\mu}\mu}(\mathbf{r}) \left[ \gamma^{(e)}(\mathbf{s}-\alpha\mathbf{r}) - \gamma^{(e)}(\mathbf{s}+\bar{\alpha}\mathbf{r}) \right], \quad (63)$$

which is odd (O) under permutation of the non-color variable of the quarks. Correspondingly, the even (E) factor in the amplitude Eq. (62) reads,

$$E_e^{\bar{\mu}\mu}(\boldsymbol{\kappa}, \mathbf{k}_T, \alpha) = \int d^2r d^2s e^{i\boldsymbol{\kappa}\cdot\mathbf{r}+i\mathbf{k}_T\cdot\mathbf{s}} \Psi_{Q\bar{Q}}^{\bar{\mu}\mu}(\mathbf{r}) \left[ \gamma^{(e)}(\mathbf{s}-\alpha\mathbf{r}) + \gamma^{(e)}(\mathbf{s}+\bar{\alpha}\mathbf{r}) - 2\gamma^{(e)}(\mathbf{s}) \right] . \quad (64)$$

Here  $\mathbf{s}$  and  $\mathbf{r}$  is the position of the center of gravity and the relative transverse separation of the  $Q\bar{Q}$  pair, respectively. It becomes evident from Eqs. (63) and (64), that the *production* amplitude for the  $Q\bar{Q}$ -pair depends on the difference between the *interaction* amplitudes represented by the three graphs in Fig. 10. For example, the two terms in the square bracket in Eq. (63) correspond to the two first graphs in Fig. 10. If the  $Q$  and the  $\bar{Q}$  would scatter at the same impact parameter, the production amplitude would vanish and nothing is produced. We stress that the interaction amplitudes represented by each of the three graphs in Fig. 10 is infrared divergent. This divergence, however, cancels in the production amplitude of the heavy quark pair, and therefore one can express the cross section for heavy flavor production in terms of color neutral quantities, such as the dipole cross section  $\sigma_{q\bar{q}}$ .

The LC wave function  $\Psi_{Q\bar{Q}}^{\bar{\mu}\mu}(\mathbf{r})$  of the  $Q\bar{Q}$  component of the incident gluon in Eqs. (63)-(64) reads,

$$\Psi_{Q\bar{Q}}^{\bar{\mu}\mu}(\mathbf{r}) = \frac{\sqrt{2\alpha_s}}{4\pi} \xi^\mu \hat{\Gamma} \tilde{\xi}^{\bar{\mu}} K_0(m_Q r) , \quad (65)$$

where the vertex operator has the form,

$$\hat{\Gamma} = m_Q \boldsymbol{\sigma} \cdot \mathbf{e} + i(1-2\alpha)(\boldsymbol{\sigma} \cdot \mathbf{n})(\mathbf{e} \cdot \boldsymbol{\nabla}) + (\mathbf{n} \times \mathbf{e}) \cdot \boldsymbol{\nabla} , \quad (66)$$

where  $\boldsymbol{\nabla} = d/d\mathbf{r}$ ;  $\alpha$  is the fraction of the gluon light-cone momentum carried by the quark  $Q$  and  $\bar{\alpha}$  is the analogous quantity for the antiquark  $\bar{Q}$ ;  $\mathbf{e}$  is the polarization vector of the gluon and  $m_Q$  is the heavy quark mass.

The profile function  $\gamma^{(e)}(\mathbf{s})$  in Eqs. (63)–(64) is related by Fourier transformation to the amplitude  $F^{(e)}(\mathbf{k}_T, \{X\})$ , of absorption of a real gluon by a nucleon,  $GN \rightarrow X$ , which also can be treated as an "elastic" (color-exchange) gluon-nucleon scattering with momentum transfer  $\mathbf{k}_T$ ,

$$\gamma^{(e)}(\mathbf{s}) = \frac{\sqrt{\alpha_s}}{2\pi\sqrt{6}} \int \frac{d^2k_T}{k_T^2 + \lambda^2} e^{-i\mathbf{k}_T\cdot\mathbf{s}} F_{GN \rightarrow X}^{(e)}(\mathbf{k}_T, \{X\}) , \quad (67)$$

where the upper index ( $e$ ) shows the color polarization of the gluon, and the variables  $\{X\}$  characterize the final state  $X$  including the color of the scattered gluon.

It is important for further consideration to relate the profile function (67) to the unintegrated gluon density  $\mathcal{F}(k_T, x)$  and to the dipole cross section  $\sigma_{q\bar{q}}(r, x)$  (*cf.* sect. 2),

$$\begin{aligned} & \int d^2b d\{X\} \sum_{e=1}^8 \left| \gamma^{(e)}(\mathbf{s} + \mathbf{r}) - \gamma^{(e)}(\mathbf{s}) \right|^2 \\ &= \frac{4\pi}{3} \alpha_s \int \frac{d^2k_T}{k_T^2} (1 - e^{i\mathbf{k}_T \cdot \mathbf{r}}) \mathcal{F}(k_T, x_2) = \sigma_{q\bar{q}}(r, x_2). \end{aligned} \quad (68)$$

Let us consider the production cross sections of a  $Q\bar{Q}$  pair in each of three states listed above, Eqs. (60)–(62). The cross section of a color-singlet  $Q\bar{Q}$  pair, averaged over polarization and colors of the incident gluon reads,

$$\sigma^{(1)} = \frac{1}{(2\pi)^4} \sum_{\mu, \bar{\mu}, i, j} \int_0^1 d\alpha \int d^2\kappa d^2k_T \left| A_{ij,a}^{\mu\bar{\mu}}(\boldsymbol{\kappa}, \mathbf{k}_T, \alpha) \right|^2 \quad (69)$$

Using Eqs. (63), (65) and (68) this relation can be modified as,

$$\sigma^{(1)} = \sum_{\mu, \bar{\mu}} \int_0^1 d\alpha \int d^2r \sigma_1(r, \alpha) \left| \Psi^{\mu\bar{\mu}}(\mathbf{r}, \alpha) \right|^2, \quad (70)$$

where

$$\sigma_1(r, \alpha) = \frac{1}{8} \sigma_{q\bar{q}}(r, x_2); \quad (71)$$

$$\sum_{\mu, \bar{\mu}} \left| \Psi^{\mu\bar{\mu}}(\mathbf{r}, \alpha) \right|^2 = \frac{\alpha_s}{(2\pi)^2} \left[ m_Q^2 K_0^2(m_Q r) + (\alpha^2 + \bar{\alpha}^2) m_Q^2 K_1^2(m_Q r) \right]. \quad (72)$$

One finds in a similar way that the cross sections of a color-octet  $Q\bar{Q}$  pair production either in  $8^-$  (Odd) or  $8^+$  (Even) states has the form,

$$\sigma_{O(E)}^{(8)} = \sum_{\mu, \bar{\mu}} \int_0^1 d\alpha \int d^2r \sigma_{O(E)}^{(8)}(r, \alpha) \left| \Psi^{\mu\bar{\mu}}(\mathbf{r}, \alpha) \right|^2, \quad (73)$$

where

$$\sigma_O^{(8)}(r, \alpha, x_2) = \frac{5}{16} \sigma_{q\bar{q}}(r, x_2); \quad (74)$$

$$\sigma_E^{(8)}(r, \alpha, x_2) = \frac{9}{16} \left[ 2\sigma_{q\bar{q}}(\alpha r, x_2) + 2\sigma_{q\bar{q}}(\bar{\alpha} r, x_2) - \sigma_{q\bar{q}}(r, x_2) \right]. \quad (75)$$

After summation over all three color states in which the  $Q\bar{Q}$  pair in Fig. 10 can be produced, one obtains for the partonic cross section [4],

$$\sigma(GN \rightarrow \{Q\bar{Q}\}X) = \int_0^1 d\alpha \int d^2r \left| \Psi_{G \rightarrow Q\bar{Q}}(\alpha, r) \right|^2 \sigma_{q\bar{q}G}(\alpha, r), \quad (76)$$

where  $\sigma_{q\bar{q}G}$  is the cross section for scattering a color neutral quark-antiquark-gluon system on a nucleon [4],

$$\sigma_{q\bar{q}G}(\alpha, r) = \frac{9}{8} [\sigma_{q\bar{q}}(\alpha r) + \sigma_{q\bar{q}}(\bar{\alpha} r)] - \frac{1}{8} \sigma_{q\bar{q}}(r). \quad (77)$$

In order to simplify the notation, we do not explicitly write out the  $x_2$  dependence of the dipole cross section.

The light-cone (LC) wavefunctions for the transition  $G \rightarrow Q\bar{Q}$  can be calculated perturbatively and are very similar to the ones in lepton production, Eq. (34),

$$\begin{aligned} \Psi_{G \rightarrow Q\bar{Q}}(\alpha, \mathbf{r}_1) \Psi_{G \rightarrow Q\bar{Q}}^*(\alpha, \mathbf{r}_2) = & \frac{\alpha_s(\mu_R)}{(2\pi)^2} \left\{ m_Q^2 K_0(m_Q r_1) K_0(m_Q r_2) \right. \\ & \left. + [\alpha^2 + \bar{\alpha}^2] m_Q^2 \frac{\mathbf{r}_1 \cdot \mathbf{r}_2}{r_1 r_2} K_1(m_Q r_1) K_1(m_Q r_2) \right\}, \end{aligned} \quad (78)$$

where  $\alpha_s(\mu_R)$  is the strong coupling constant, which is probed at a renormalization scale  $\mu_R \sim m_Q$ .

Eq. (76) is a special case of the general rule that at high energy, the cross section for the reaction  $a + N \rightarrow \{b, c, \dots\} X$  can be expressed as convolution of the LC wavefunction for the transition  $a \rightarrow \{b, c, \dots\}$  and the cross section for scattering the color neutral  $\{\text{anti-}a, b, c, \dots\}$ -system on the target nucleon  $N$ .

Note that although the dipole cross section is flavor independent, the integral Eq. (76) is not. Since the Bessel functions  $K_{1,0}$  decay exponentially for large arguments, the largest values of  $r$  which can contribute to the integral are of order  $\sim 1/m_Q$ . We point out, that as a consequence of color transparency [13,22], the dipole cross section vanishes  $\propto r^2$  for small  $r$ . Therefore, the  $Q\bar{Q}$  production cross section behaves roughly like  $\propto 1/m_Q^2$  (modulo logs and saturation effects).

We can estimate the relative yield of the  $1^-$ ,  $8^-$  and  $8^+$  states we can rely upon the approximation  $\sigma_{q\bar{q}}(r) \propto r^2$  which is rather accurate in the case of a  $Q\bar{Q}$  pair, since its separation  $r \sim 1/m_Q$  is small. We then derive,

$$\sigma^{(1)} : \sigma_O^{(8)} : \sigma_E^{(8)} = 1 : \frac{5}{2} : \frac{117}{70}. \quad (79)$$

Thus, about 20% of the produced  $Q\bar{Q}$  pairs are in a color-singlet state, the rest are color-octets.

In order to calculate the cross section for heavy quark pair production in  $pp$  collisions, Eq. (76) has to be weighted with the projectile gluon density,

$$\frac{d\sigma(pp \rightarrow \{Q\bar{Q}\}X)}{dy} = x_1 G(x_1, \mu_F) \sigma(GN \rightarrow \{Q\bar{Q}\}X), \quad (80)$$

where  $y = \frac{1}{2} \ln(x_1/x_2)$  is the rapidity of the pair and  $\mu_F \sim m_Q$ . In analogy to the parton model, we call  $\mu_F$  the factorization scale. Uncertainties arising from the choice of this scale will be investigated in section 6.1. Integrating over all kinematically allowed rapidities yields

$$\sigma_{\text{tot}}(pp \rightarrow \{Q\bar{Q}\}X) = 2 \int_0^{-\ln(\frac{2m_Q}{\sqrt{s}})} dy x_1 G(x_1, \mu_F) \sigma(GN \rightarrow \{Q\bar{Q}\}X). \quad (81)$$

A word of caution is in order, regarding the limits of the  $\alpha$ -integration in Eq. (76). Since the invariant mass of the  $Q\bar{Q}$ -pair is given by

$$M_{Q\bar{Q}}^2 = \frac{\kappa_{\perp}^2 + m_Q^2}{\alpha\bar{\alpha}}, \quad (82)$$

the endpoints of the  $\alpha$ -integration include configurations corresponding to arbitrarily large invariant masses, eventually exceeding the total available  $cm$ . energy. However, since  $r$  and  $\kappa_{\perp}$  (the single quark transverse momentum) are conjugate variables, the pair mass is not defined in the mixed representation, nor are the integration limits for  $\alpha$ . Fortunately, this problem is present only at the very edge of the phase space and therefore numerically negligible.

### 6.1 Numerical results for hadroproduction of heavy quarks

Still the questions remain, how well does the dipole approach describe experimental data. Since there are not many data for the total cross section, we shall also compare predictions from the dipole approach to calculations in the NLO parton model [60–62]<sup>2</sup> For  $\sigma_{q\bar{q}}$ , we use an improved version of the saturation model presented in Ref. [28], which now also includes DGLAP evolution [63]. This improvement has no effect on open charm, but is important for bottom production.

In the dipole approach, we use the one loop running coupling constant,

$$\alpha_s(\mu_R) = \frac{4\pi}{\left(11 - \frac{2}{3}N_f\right) \ln\left(\frac{\mu_R^2}{(200 \text{ MeV})^2}\right)} \quad (83)$$

at a renormalization scale  $\mu_R \sim m_Q$ , and the number of light flavors is chosen to be  $N_f = 3$  for open charm and  $N_f = 4$  for open bottom production. Furthermore, we use the GRV98LO [64] gluon distribution to model the gluon density in the projectile. We use a leading order parton distribution function (PDF), because of its probabilistic interpretation. Note that one could attempt to calculate the projectile gluon distribution from the dipole cross section. However, the projectile distribution functions are needed mostly at large momentum fraction  $x_1$ , where the dipole cross section is not constrained by data.

Our results for the total charm pair cross section in proton-proton ( $pp$ ) collisions is shown in Fig. 11 as function of center of mass energy. The left panel shows the uncertainties of both approaches by varying quark mass  $m_c$  and renormalization scale  $\mu_R$  in the intervals  $1.2 \text{ GeV} \leq m_c \leq 1.8 \text{ GeV}$  and  $m_c \leq \mu_R \leq 2m_c$ , respectively. The factorization scale is kept fixed at  $\mu_F = 2m_c$ , because in our opinion, the charm quark mass is too low for DGLAP evolution. A large fraction of the resulting uncertainty originates from different possible choices of the charm quark mass, since the total cross section behaves approximately like  $\sigma_{\text{tot}} \propto m_Q^{-2}$ .

<sup>2</sup> A FORTRAN program for the NLO parton model calculation is available at <http://n.home.cern.ch/n/nason/www/hvqlib.html>.

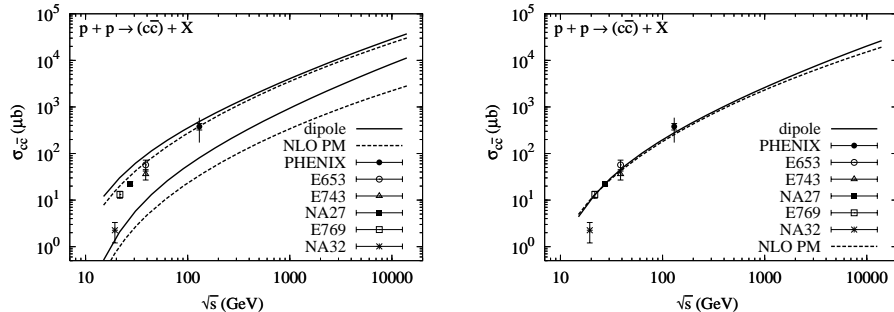


**Fig. 11.** Results for the total open charm pair cross section as function of cm. energy. Varying free parameters in dipole approach (solid lines) and in the parton model (dashed lines) gives rise to the uncertainties shown on the left. In the figure on the right, parameters in both models have been adjusted so that experimental data [65,66] are described.

Note that the mean value of  $x_2$  increases with decreasing energy. At  $\sqrt{s} = 130$  GeV one has  $x_2 \sim 0.01$ . For lower energies, our calculation is an extrapolation of the saturation model. For the highest fixed target energies of  $\sqrt{s} \approx 40$  GeV, values of  $x_2 \sim 0.1$  become important. Unlike in the Drell-Yan case, which was studied in [6], the dipole approach to heavy quark production does not show any unphysical behavior when extrapolated to larger  $x_2$ . One reason for this is that the new saturation model [63] assumes a realistic behavior of the gluon density at large  $x_2$ . In addition, even at energies as low as  $\sqrt{s} = 15$  GeV, the gluon-gluon fusion process is the dominant contribution to the cross section.

Because of the wide uncertainty bands, one can adjust  $m_c$  and  $\mu_R$  in both approaches so that experimental data are reproduced. Then, dipole approach and NLO parton model yield almost identical results. However, the predictive power of the theory is rather small. In Fig. 11 (right), we used  $m_c = 1.2$  GeV and  $\mu_R = 1.5m_c$  for the NLO parton model calculation and  $m_c = 1.4$  GeV,  $\mu_R = m_c$  in the dipole approach. The data points tend to lie at the upper edge of the uncertainty bands, so that rather small values of  $m_c$  are needed to describe them.

There are remaining uncertainties which are not shown in Fig. 11 (right), because different combinations of  $m_c$  and  $\mu_R$  can also yield a good description of the data. In addition, different PDFs will lead to different values of the cross section at high energies, since the heavy quark cross section is very sensitive to the low- $x$  gluon distribution. In [67], it was found that an uncertainty of a factor of  $\sim 2.3$  remains at  $\sqrt{s} = 14$  TeV (in the NLO parton model), even after all free parameters had been fixed to describe total cross section data at lower energies. It is interesting to see that 20 – 30% of the total  $pp$  cross section at LHC ( $\sqrt{s} = 14$  TeV) goes into open charm <sup>3</sup>.

<sup>3</sup> The Donnachie-Landshoff parameterization of the total  $pp$  cross section [68] predicts  $\sigma_{\text{tot}}^{pp}(\sqrt{s} = 14 \text{ TeV}) = 100$  mb.

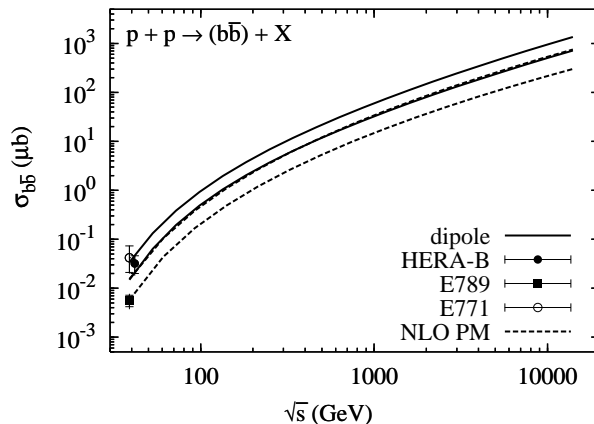


**Fig. 12.** *Uncertainties of open  $b\bar{b}$  pair production calculated in the dipole approach (solid) and in the NLO parton model (dashed). The dipole approach seems to provide a better description of the data, even though HERA-B energy is too low for the dipole approach.*

Next, we calculate the total  $b\bar{b}$ -pair cross section as function of center of mass energy, see Fig. 12. In order to quantify the theoretical uncertainties, we vary the free parameters over the ranges  $4.5 \text{ GeV} \leq m_b \leq 5 \text{ GeV}$  and  $m_b \leq \mu_R, \mu_F \leq 2m_b$ . Because of the large  $b$ -quark mass, uncertainties are much smaller than for open charm production. One can see that the dipole approach tends to predict higher values than the NLO parton model, even though the energy dependence expected in both approaches is very similar. In fact, the results calculated in the dipole approach with  $m_b = 5 \text{ GeV}$  agree almost exactly with the NLO parton model calculation with  $m_b = 4.5 \text{ GeV}$ . For all other values of  $m_b$ , the uncertainty bands of the two approaches do not overlap, in contrast to the case for open charm production.

Three measurements of open  $b\bar{b}$  production are published in the literature [69–71]. The two values of the open bottom cross section measured at Fermilab [69,70] at  $cm.$  energy  $\sqrt{s} = 38.8 \text{ GeV}$  differ by almost three standard deviations. The HERA-B measurement at slightly larger  $cm.$  energy  $\sqrt{s} = 41.6 \text{ GeV}$  [71] is consistent with the E771 [70] value. These two points seem to be better described by the dipole approach, though the NLO parton model (with  $m_b = 4.5 \text{ GeV}$ ) still touches the HERA-B error bar. Note that also a different set of PDFs would not significantly pull up the parton model curve [67], as a lower value of the  $b$ -quark mass would do. With a resummation of terms from higher order corrections [72], however, the parton model can reproduce each of the three measurements within theoretical uncertainties, see Ref. [71]. On the other hand, typical values of  $x_2$  which are important for  $b\bar{b}$  production at HERA-B energy are of order  $x_2 \sim 0.2$ , while the parameterization [63] of the dipole cross section is constrained only by DIS data with  $x_{Bj} \leq 0.01$ .

While it is an advantage of the dipole formulation to provide very simple formulas that allow one to absorb much of the higher order corrections into a phenomenological parameterization of  $\sigma_{q\bar{q}}(x_2, r)$ , one cannot clarify the origin of the discrepancy in normalizations without a systematic calculation of higher orders in this approach.

## 7 Nuclear effects in hadroproduction of open charm

It is still unclear whether available data from fixed target experiments demonstrate any nuclear effects for open charm production [73–75]. Naively one might expect no effects at all, since a heavy quark should escape the nucleus without attenuation or reduction of its momentum. In fact, this is not correct even at low energies as is explained below. Moreover, at high energies one cannot specify any more initial or final state interactions. The process of heavy flavor production takes a time interval longer than the nuclear size, and the heavy quarks are produced coherently by many nucleons which compete with each other. As a result the cross section is reduced, and this phenomenon is called shadowing.

In terms of parton model the same effect is interpreted in the infinite momentum frame of the nucleus as reduction of the nuclear parton density due to overlap and fusion of partons at small Bjorken  $x$ . The kinematic condition for overlap is the same as for coherence in the nuclear rest frame. Thus, heavy quark via gluon fusion can be shadowed in the leading twist, if the gluon density in nuclei is reduced due to gluon shadowing.

There are well known examples of shadowing observed in hard reactions, like deep-inelastic scattering (DIS) [76] and the Drell-Yan process (DY) [77] demonstrating a sizable reduction of the density of light sea quarks in nuclei. Shadowing is expected also for gluons, although there is still no experimental evidence for that.

Shadowing for heavy quarks is a higher twist effect, and although its magnitude is unknown within the standard parton model approach, usually it is neglected for charm and beauty production. However, this correction is proportional to the gluon density in the proton and steeply rises with energy. Unavoidably, such a correction should become large at high energies. In some instances, like for charmonium production, this higher twist effect gains a large numerical factor and leads to a rather strong suppression even at energies of fixed target experiments (see below).

On the other hand, gluon shadowing which is a leading twist effect, is expected to be the main source of nuclear suppression for heavy flavor production at high energies. This is why this process is usually considered as a sensitive probe for the gluon density in hadrons and nuclei. If one neglects terms suppressed by a power of  $1/m_Q^2$ , the cross section of heavy  $Q\bar{Q}$  production in  $pA$  collision is suppressed by the gluon shadowing factor  $R_A^G$  compared to the sum of  $A$  nucleon cross sections,

$$\sigma_{pA}^{Q\bar{Q}}(x_1, x_2) = R_A^G(x_1, x_2) A \sigma_{pN}^{Q\bar{Q}}(x_1, x_2) . \quad (84)$$

Here

$$R_A^G(x_1, x_2) = \frac{1}{A} \int d^2b R_A^G(x_1, x_2, b) T_A(b) , \quad (85)$$

where  $R_A^G(x_1, x_2, b)$  is the (dimensional) gluon shadowing factor at impact parameter  $b$ ;  $T_A(b) = \int_{-\infty}^{\infty} dz \rho_A(b, z)$  is the nuclear thickness function, and  $x_1, x_2$  are the Bjorken variables of the gluons participating in  $Q\bar{Q}$  production from the colliding proton and nucleus.

The parton model cannot predict shadowing, but only its evolution at high  $Q^2$ , while the main contribution originates from the soft part of the interaction. The usual approach is to fit data at different values of  $x$  and  $Q^2$  employing the DGLAP evolution and fitting the distributions of different parton species parametrized at some intermediate scale [78,79]. However, the present accuracy of data for DIS on nuclei do not allow to fix the magnitude of gluon shadowing, which is found to be compatible with zero<sup>4</sup>. Nevertheless, the data exclude some models with too strong gluon shadowing [80].

Another problem faced by the parton model is the impossibility to predict gluon shadowing effect in nucleus-nucleus collisions even if the shadowing factor Eq. (84) in each of the two nuclei was known. Indeed, the cross section of  $Q\bar{Q}$  production in collision of nuclei  $A$  and  $B$  at impact parameter  $\mathbf{b}$  reads,

$$\frac{d\sigma_{AB}^{Q\bar{Q}}(x_1, x_2)}{d^2b} = R_{AB}^G(x_1, x_2, b) AB \sigma_{NN}^{Q\bar{Q}}(x_1, x_2) , \quad (86)$$

where

$$R_{AB}^G(x_1, x_2, b) = \frac{1}{AB} \int d^2s R_A^G(x_1, \mathbf{s}) T_A(s) R_B^G(x_2, \mathbf{b} - \mathbf{s}) T_B(\mathbf{b} - \mathbf{s}) . \quad (87)$$

In order to calculate the nuclear suppression factor Eq. (87) one needs to know the impact parameter dependence of gluon shadowing,  $R_A^G(x_1, \mathbf{b})$ , while only integrated nuclear shadowing Eq. (85) can be extracted from lepton- or hadron-nucleus data<sup>5</sup>. Note that the parton model prediction of shadowing effects for minimum bias events integrated over  $b$  suffers the same problem. Apparently, QCD factorization cannot be applied to heavy ion collisions even at large scales. The same is true for quark shadowing expected for Drell-Yan process in heavy ion collisions [15,54,81].

Nuclear shadowing can be predicted within the light-cone (LC) dipole approach which describes it via simple eikonalization of the dipole cross section. It was pointed out in Ref. [13] that quark configurations (dipoles) with fixed transverse separations are the eigenstates of interaction in QCD, therefore eikonalization is an exact procedure. In this way one effectively sums up the Gribov's inelastic corrections to all orders [13].

<sup>4</sup> Gluon shadowing was guessed in [78] to be the same as for  $F_2(x, Q^2)$  at the semi-hard scale.

<sup>5</sup> One can get information on the impact parameter of particle-nucleus collision measuring multiplicity of produced particles or low energy protons (so called grey tracks). However, this is still a challenge for experiment.



The advantage of this formalism is that it does not need any  $K$ -factor. Indeed, it was demonstrated recently in Ref. [6] that the simple dipole formalism for Drell-Yan process [15,82,83] precisely reproduces the results of very complicated next-to-leading calculations at small  $x$ . The LC dipole approach also allows to keep under control deviations from QCD factorization. In particular, we found a substantial process-dependence of gluon shadowing due to the existence of a semi-hard scale imposed by the strong nonperturbative interaction of light-cone gluons [29]. For instance gluon shadowing for charmonium production off nuclei was found in Ref. [2] to be much stronger than in deep-inelastic scattering [29].

The LC dipole approach also provides effective tools for calculation of transverse momentum distribution of heavy quarks, like it was done for radiated gluons in Ref. [83,84], or Drell-Yan pairs in Ref. [54]. Nuclear broadening of transverse momenta of the heavy quarks also is an effective way to access the nuclear modification of the transverse momentum distribution of gluons, *i.e.* the so called phenomenon of color glass condensate or gluon saturation [85,86]. We consider only integrated quantities here.

In what follows we find sizable deviations from QCD factorization for heavy quark production off nuclei. First of all, for open charm production shadowing related to propagation of a  $c\bar{c}$  pair through a nucleus is not negligible, especially at the high energies of RHIC and LHC, in spite of smallness of  $c\bar{c}$  dipoles. Further, higher Fock components containing gluons lead to gluon shadowing which also deviates from factorization and depends on quantum numbers of the produced heavy pair  $c\bar{c}$ .

### 7.1 Higher twist shadowing for $c\bar{c}$ production

An important advantage of the LC dipole approach is the simplicity of calculations of nuclear effects. Since partonic dipoles are the eigenstates of interaction one can simply eikonalize the cross section on a nucleon target [13] provided that the dipole size is “frozen” by Lorentz time dilation. Therefore, the cross section of a  $c\bar{c}$  pair production off a nucleus has the form [59,4],

$$\sigma(GA \rightarrow c\bar{c}X) = 2 \sum_{\mu, \bar{\mu}} \int d^2b \int d^2r \int_0^1 d\alpha \left| \Psi^{\mu\bar{\mu}}(\mathbf{r}, \alpha) \right|^2 \times \left\{ 1 - \exp \left[ -\frac{1}{2} \sigma_{q\bar{q}G}(r, \alpha, x_2) T_A(b) \right] \right\}, \quad (88)$$

where  $\sigma_{q\bar{q}G}(r, \alpha, x_2)$  is the cross section of interaction of a  $c\bar{c}G$  three particle state with a nucleon, see sect. 6.

Apparently, this expression leads to shadowing correction which is a higher twist effect and vanishes as  $1/m_c^2$ . Indeed, it was found in [59] that in the kinematic range of fixed target experiments at the Tevatron, Fermilab,  $x_2 \sim 10^{-2}$ ,  $x_F \sim 0.5$ , the shadowing effects are rather weak even for heavy nuclei,

$$1 - R_A \lesssim 0.05, \quad (89)$$

where  $R_A$  is defined in (84).

On the other hand, a substantial shadowing effect, several times stronger than in Eq. (89) was found in Ref. [2] for charmonium production (see below), although it is also a higher twist effect. In the case of open charm production there are additional cancelations which grossly diminish shadowing. The smallness of the effect maybe considered as a justification for the parton model prescription to neglect this correction as a higher twist effect. However, the dipole cross section  $\sigma_{q\bar{q}}(r, x_2)$  steeply rises with  $1/x_2$  especially at small  $r$  and the shadowing corrections increase, reaching values of about 10% at  $x_2 = 10^{-3}$ , and about 30% at  $x_2 = 10^{-5}$ .

## 7.2 Process dependent gluon shadowing

The phenomenological dipole cross section which enters the exponent in Eq. (88) is fitted to DIS data. Therefore it includes effects of gluon radiation which are in fact the source of rising energy ( $1/x$ ) dependence of the  $\sigma_{q\bar{q}}(r, x)$ . However, a simple eikonalization in Eq. (88) corresponds to the Bethe-Heitler approximation assuming that the whole spectrum of gluons is radiated in each interaction independently of other rescatterings. This is why the higher order terms in expansion of (88) contain powers of the dipole cross section. However, gluons radiated due to interaction with different bound nucleons can interfere leading to damping of gluon radiation similar to the Landau-Pomeranchuk [87] effect in QED. Therefore, the eikonal expression Eq. (88) needs corrections which are known as gluon shadowing.

Nuclear shadowing of gluons is a leading twist effect since the cloud of massless gluons has a larger size than the source which is a small size  $barcc$  pair. Gluon shadowing is treated by the parton model in the infinite momentum frame of the nucleus as a result of glue-gluon fusion. On the other hand, in the nuclear rest frame the same phenomenon is expressed in terms of the Glauber like shadowing for the process of gluon radiation [88]. In impact parameter representation one can easily sum up all the multiple scattering corrections which have the simple eikonal form [13]. Besides, one can employ the well developed color dipole phenomenology with parameters fixed by data from DIS. Gluon shadowing was calculated employing the light-cone dipole approach for DIS [29] and production of charmonia [2], and a substantial deviation from QCD factorization was found. Here we calculate gluon shadowing for  $c\bar{c}$  pair production.

First of all, one should develop a dipole approach for gluon radiation accompanying production of a  $c\bar{c}$  pair in gluon-nucleon collision. Then nuclear effects can be easily calculated via simple eikonalization. This is done in Ref. [4].

According to the general prescription [15] the dipole cross section which enters the factorized formula for the process of parton  $a$ -nucleon collision leading to multiparton production,  $a N \rightarrow b + c + \dots + d X$ , is the cross section for the colorless multiparton ensemble  $|\bar{a}bc\dots d\rangle$ . The same multiparton dipole cross section is responsible for nuclear shadowing. Indeed, in the case of the process  $GN \rightarrow c\bar{c}X$  it was the cross section  $\sigma_{q\bar{q}G}$ , Eq. (77), which correspond to a state  $|c\bar{c}G\rangle$  interacting with a nucleon.

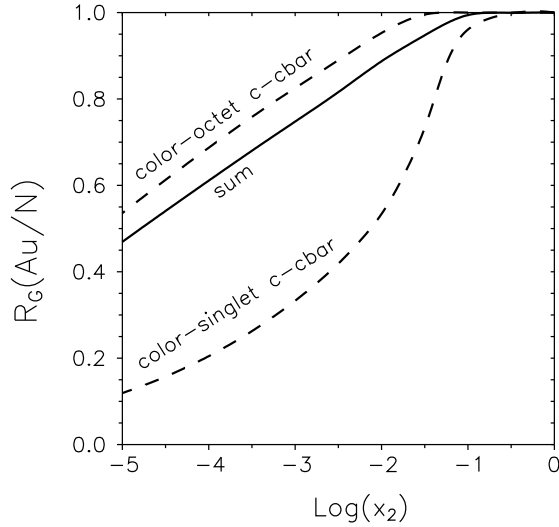


**Fig. 13.** Ratio of gluon densities  $R_G(Au/p) = G_{Au}(x_2)/195 G_p(x_2)$  for color octet-octet and singlet-octet states ( $c\bar{c}$ ) –  $G$  (dashed curves). The averaged gluon shadowing is depicted by the solid curve.

Correspondingly, in the case of additional gluon production,  $G \rightarrow \bar{c}cG$ , it is a 4-parton,  $|\bar{c}cGG\rangle$ , cross section  $\sigma_4(\mathbf{r}, \boldsymbol{\rho}, \alpha_1, \alpha_2, \alpha_3)$ . Here  $\mathbf{r}$  and  $\boldsymbol{\rho}$  are the transverse  $c\bar{c}$  separation and the distance between the  $c\bar{c}$  center of gravity and the final gluon, respectively. Correspondingly,  $\alpha_1 = \alpha_c$ ,  $\alpha_2 = \alpha_{\bar{c}}$ , and  $\alpha_3 = \alpha_G$ . Treating the charm quark mass as a large scale, one can neglect  $r \ll \rho$ , then the complicated expression for  $\sigma_4$  becomes rather simple. One can find details in Ref. [4].

One can treat partons as free only if their transverse momenta are sufficiently large, otherwise the nonperturbative interaction between partons may generate power corrections [29]. Apparently, the softer the process is, the more important are these corrections. In particular, diffraction and nuclear shadowing are very sensitive to these effects. Indeed, the cross section of diffractive dissociation to large masses (so called triple-Pomeron contribution) is proportional to the fourth power of the size of the partonic fluctuation. Therefore, the attractive nonperturbative interaction between the partons squeezes the fluctuation and can substantially reduce the diffractive cross section. Smallness of the transverse separation in the quark-gluon fluctuation is the only known explanation for the observed suppression of the diffractive cross section, which is also known as the problem of smallness of the triple-Pomeron coupling. While no data sensitive to gluon shadowing are available yet, a vast amount of high accuracy diffraction data can be used to fix the parameters of the nonperturbative interaction.

It turns out [4] that the color interaction between the gluon and the  $c\bar{c}$  pair depends on color states of the latter. If the  $c\bar{c}$  pair is in one of the two color octet states, the nonperturbative interaction between the pair and the gluon is strong, and the  $|q\bar{q}G\rangle$  system cannot become larger than a typical constituent quark radius  $\sim 0.3$  fm. For these small configurations, shadowing is rather small, see Fig. 13. If, on the other hand, the  $c\bar{c}$  pair is in a color singlet state, the color charges of the  $c$  and the  $\bar{c}$  screen each other, so that the pair cannot interact strongly with the radiated gluon, *i.e.* the value of  $b_0$  (see sect. 5.2) is much smaller than 0.65 GeV. The transverse size of these configurations is limited only by confinement, hence they can become as large as a typical hadron. Therefore, gluon shadowing is much stronger in the color singlet channel [2].

### 7.3 Numerical results

To observe the shadowing effects in open charm production, one must access the kinematic region of sufficiently small  $x_2 \lesssim 0.1$ . With fixed targets it can be achieved at highest energies at Fermilab and in the experiment HERA-B at DESY. We apply the results of the previous section for gluon shadowing to  $c\bar{c}$  pair production in proton-nucleus collisions. We assume that the  $c\bar{c}$  is produced with Feynman  $x_F$  corresponding to  $x_2 = (-x_F + \sqrt{x_F^2 + 4M_{c\bar{c}}^2/s})/2$ , where we fix  $M_{c\bar{c}} = 4$  GeV. The contribution of gluon shadowing to nuclear effects in proton-tungsten collision at  $p_{lab} = 900$  GeV is depicted by the dashed curve in Fig. 14.

The higher twist shadowing correction, which corresponds to the eikonized dipole cross section  $\sigma_{q\bar{q}G}$  in Eq. (88), is also a sizable effect and should be added. It is diminished, however, due to the strong gluon shadowing which also reduces the amount of gluons available for multiple interactions compared to the eikonal approximation Eq. (88). We take this reduction into account multiplying  $\sigma_{q\bar{q}G}$  in Eq. (88) by  $R_G(x_2, M_{c\bar{c}})$ . This procedure is justified at small transverse separations, since  $\sigma(r, x) = (\pi^2/3) \alpha_s / r^2 G(x, Q^2 \sim 1/r^2)$  [45]. For large separations see discussion in Ref. [2]. The summed shadowing suppression of  $c\bar{c}$  production is depicted in Fig. 14 by the solid curve.

Besides shadowing, other nuclear effects are possible. The EMC effect, suppression of the nuclear structure function  $F_2^A(x, Q^2)$  at large  $x$ , as well as the enhancement at  $x \sim 0.1$  should also lead to similar modifications in the gluon distribution function  $G^A(x, Q^2)$ . These effects are different from shadowing which is a result of coherence. A plausible explanation relates them with medium effects, like swelling of bound nucleons [89]. To demonstrate a possible size of the medium effects on gluon distribution we parametrize and apply the effect of gluon enhancement and suppression at large  $x$  suggested in Ref. [78]. Although it is based on ad hoc gluon shadowing and underestimated shadowing for valence quarks (see discussion in Ref. [54]), it demonstrates the scale of possible effects missed in our analysis.

There are still other effects missed in our calculations. At this energy, the effect of energy loss due to initial state interactions [90] causes additional nuclear suppression at large  $x_F$  (compare with Ref. [2]). Another correction is related to

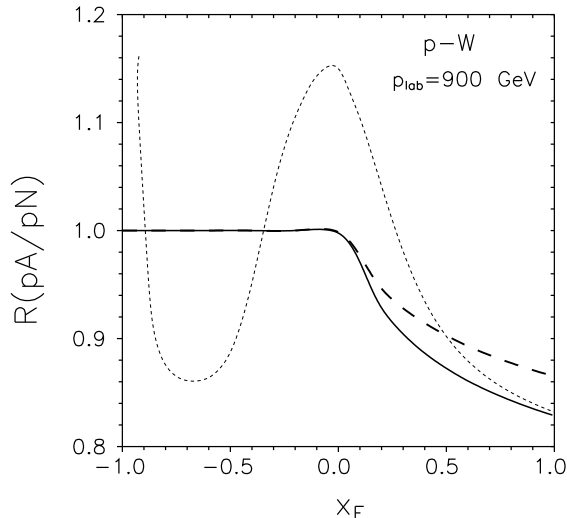


**Fig. 14.** Nuclear effects for open charm production in  $p - W$  collisions at 900 GeV beam energy. The contribution of gluon shadowing is shown by dashed curve. The solid curve represents the full shadowing effect including the higher twist contribution given by Eq. (88). Possible medium effects including antishadowing and EMC-suppression for gluons [78] are also added and the result is represented by the dotted curve.

the observation that detection of a charm hadron at large  $|x_F|$  does not insure that it originates from a charm quark produced perturbatively with the same  $x_F$ . Lacking gluons with  $x_{1,2} \rightarrow 1$  one can produce a fast charm hadron via a fast projectile (usually valence) quark which picks up a charm quark created at smaller  $|x_F|$ . This is actually the mechanism responsible for the observed  $D/\bar{D}$  asymmetry. It provides a rapidity shift between the parent charm quark and the detected hadron. Therefore, it may reduce shadowing effects at largest  $|x_F|$ . We leave this problem open for further study.

To predict shadowing effects in heavy ion collisions we employ QCD factorization, which we apply only for a given impact parameter. For minimal bias events

$$R_{AB}(y) = R_A(x_1) R_B(x_2) , \quad (90)$$

where  $y = \ln(x_1/x_2)/2$  is the rapidity of the  $c\bar{c}$  pair. Our predictions for RHIC ( $\sqrt{s} = 200$  GeV) and LHC ( $\sqrt{s} = 5500$  GeV) are depicted in Fig. 15 separately for net gluon shadowing (dashed curves) and full effect including higher twist quark shadowing (solid curves). Although shadowing of charmed quarks is a higher twist effect, its contribution is about 10% at RHIC and rises with energy.

One might be surprised by the substantial magnitude of shadowing expected at the energy of RHIC. Indeed, the value of  $x_{1,2} \approx 0.02$  at mid-rapidity is rather

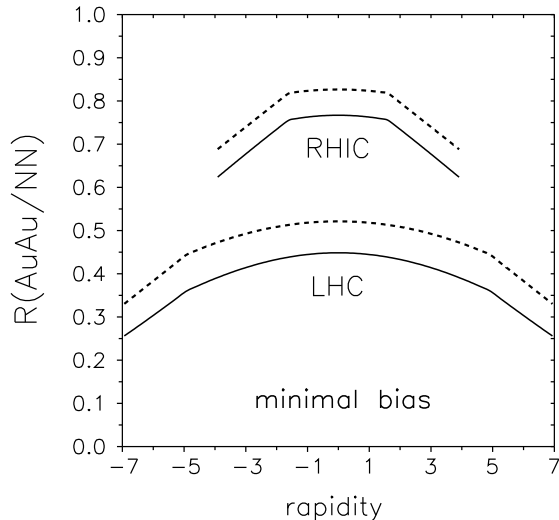


**Fig. 15.** Nuclear shadowing for open charm production in minimal bias gold-gold collision. Dotted curves show the net effect of gluon shadowing, while solid curves include both effects of gluon shadowing and the higher twist correction related to the nonzero separation of the  $c\bar{c}$ . The top (RHIC) and bottom (LHC) curves correspond to  $\sqrt{s} = 200$  GeV and 5500 GeV respectively.

large, and no gluon shadowing would be expected for DIS [29]. However, the process of charm production demonstrates a precocious onset of gluon shadowing as was discussed above. Besides, the nuclear suppression is squared in  $AA$  collisions.

Another interesting observation made in Ref. [4] is that shadowing is the same for central and minimal bias events. This has indeed been observed (within large error bars) by the PHENIX experiment [66].

## 8 The light-cone dipole formalism for charmonium production off a nucleon

The important advantage of the light-cone (LC) dipole approach is its simplicity in the calculations of nuclear effects. It has been suggested two decades ago [13] that quark configurations (dipoles) with fixed transverse separations are the eigenstates of interaction in QCD. Therefore the amplitude of interaction with a nucleon is subject to eikonalization in the case of a nuclear target. In this way one effectively sums the Gribov's inelastic corrections in all orders.

Assuming that the produced  $c\bar{c}$  pair is sufficiently small so that multigluon vertices can be neglected, we can write the cross section for  $GN \rightarrow \chi X$  as (see

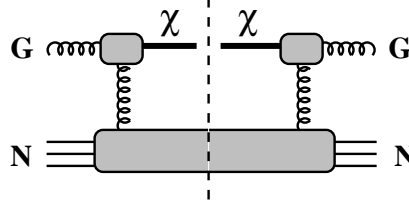


**Fig. 16.** Perturbative QCD mechanism of production of the  $\chi$  states in a gluon-nucleon collision.

Fig. 16),

$$\sigma(GN \rightarrow \chi X) = \frac{\pi}{2(N_c^2 - 1)} \sum_{a,b} \int \frac{d^2 k_T}{k_T^2} \alpha_s(k_T^2) \mathcal{F}(x, k_T^2) |M_{ab}(\mathbf{k}_T)|^2, \quad (91)$$

where  $\mathcal{F}(x, k_T^2) = \partial G(x, k_T^2) / \partial(k_T^2)$  is the unintegrated gluon density,  $G(x, k_T^2) = x g(x, k_T^2)$  ( $x = M_\chi^2 / \hat{s}$ );  $M_{ab}(\mathbf{k}_T)$  is the fusion amplitude  $GG \rightarrow \chi$  with  $a, b$  being the gluonic indices.

In the rest frame of the nucleon the amplitude can be represented in terms of the  $c\bar{c}$  LC wave functions of the projectile gluon and ejectile charmonium,

$$M_{ab}(\mathbf{k}_T) = \frac{\delta_{ab}}{\sqrt{6}} \int_0^1 d\alpha \int d^2 r \sum_{\bar{\mu}\mu} \left( \Phi_\chi^{\bar{\mu}\mu}(\mathbf{r}, \alpha) \right)^* [e^{i\mathbf{k}_T \cdot \mathbf{r}_1} - e^{i\mathbf{k}_T \cdot \mathbf{r}_2}] \Phi_G^{\bar{\mu}\mu}(\mathbf{r}, \alpha), \quad (92)$$

where

$$\mathbf{r}_1 = (1 - \alpha) \mathbf{r}, \quad \mathbf{r}_2 = -\alpha \mathbf{r}. \quad (93)$$

For the sake of simplicity, we separate the color parts  $\langle c\bar{c}, \{8\}_a |$  and  $\langle c\bar{c}, \{1\} |$  from the LC wave function of the gluon and charmonium respectively, and calculate the matrix element,

$$\langle c\bar{c}, \{8\}_a | \frac{1}{2} \lambda_b | c\bar{c}, \{1\} \rangle = \frac{\delta_{ab}}{\sqrt{6}}, \quad (94)$$

which is shown explicitly in Eq. (92). Thus, the functions  $\Phi_{G(\chi)}^{\bar{\mu}\mu}(\mathbf{r}, \alpha)$  in Eq. (92) represent only the spin- and coordinate dependent parts of the corresponding full wave functions.

The gluon wave function differs only by a factor from the photon one,

$$\Phi_G^{\bar{\mu}\mu}(\mathbf{r}, \alpha) = \frac{\sqrt{2\alpha_s}}{4\pi} \left( \xi_c^\mu \right)^\dagger \hat{O} \tilde{\xi}_c^{\bar{\mu}} K_0(\epsilon r), \quad (95)$$

where  $\xi_c^\mu$  is the  $c$ -quark spinor, and

$$\tilde{\xi}_c^{\bar{\mu}} = i \sigma_y \xi_c^{\bar{\mu}*}, \quad (96)$$

$$\hat{O} = m_c \boldsymbol{\sigma} \cdot \mathbf{e} + i(1 - 2\alpha) (\boldsymbol{\sigma} \cdot \mathbf{n}) (\mathbf{e} \cdot \nabla) + (\mathbf{e} \times \mathbf{n}) \nabla, \quad (97)$$

$$\begin{aligned}\epsilon^2 &= Q^2\alpha(1-\alpha) + m_c^2, \\ \nabla &= \frac{d}{d\mathbf{r}}.\end{aligned}\tag{98}$$

The gluon has virtuality  $Q^2$  and polarization vector  $\mathbf{e}$  and is moving along the unit vector  $\mathbf{n}$  (in what follows we consider only transversely polarized gluons,  $\mathbf{e} \cdot \mathbf{n} = 0$ ).

The expression for the LC wave function of a charmonium and the wavefunction of the charmonium in its rest frame are related in a somewhat complicated way by Lorentz transformation, as discussed in sect. 4. This complexity is a consequence of the nonlocal relation between the LC variables  $(\mathbf{r}, \alpha)$  and the components of the 3-dimensional relative  $c\bar{c}$  radius-vector in the rest frame of the charmonium. Also the Melosh spin rotation leads to a nontrivial relations between the two wave functions (see *e.g.* in [1]). This is a relativistic effect, it vanishes in the limit of small velocity  $v \rightarrow 0$  of the quarks in the charmonium rest frame.

A word of caution is in order. In some cases the Melosh spin rotation is important even in the limit of vanishing quark velocity  $v \rightarrow 0$ . An example is the Landau-Yang theorem [91] which forbids production of the  $\chi_1$  state by two massless gluons. However, the LC approach leads to creation of the  $\chi_1$  even in the limit  $v \rightarrow 0$  if the effect of spin rotation is neglected. It is demonstrated in Ref. [2] that the Landau-Yang theorem is restored only if the Melosh spin rotation is included. Such a cancelation of large values is a kind of fine tuning and is a good support for the procedure of Lorentz boosting which we apply to the charmonium wave functions.

Since the gluon LC wave function smoothly depends on  $\alpha$  while the charmonium wave function peaks at  $\alpha = 1/2$  with a tiny width estimated in Ref. [2],  $\langle(\alpha - 1/2)^2\rangle = 0.01$ , we can replace the charmonium wave function in the matrix element in Eq. (92) with

$$\Phi_\chi^{\bar{\mu}\mu}(r, \alpha) \approx \delta\left(\alpha - \frac{1}{2}\right) \int d\alpha \Phi_\chi^{\bar{\mu}\mu}(r, \alpha).\tag{99}$$

It is convenient to expand the LC charmonium wave function in powers of  $v$ . The result depends on the total momentum  $J$  and its projection  $J_z$  on the direction  $\mathbf{n}$ . The charmonium wave function integrated over  $\alpha$  has the form,

$$\begin{aligned}\int d\alpha \Phi_\chi^{\bar{\mu}\mu}(r, \alpha) &= (\xi^\mu)^\dagger \left[ \boldsymbol{\sigma} \cdot \mathbf{e}_\pm + \frac{1}{m} (\mathbf{e}_\pm \times \mathbf{n}) \cdot \nabla \right. \\ &\quad \left. - \frac{1}{2m_c^2} (\mathbf{e}_\pm \cdot \nabla) (\boldsymbol{\sigma} \cdot \nabla) \right] \tilde{\xi}^{\bar{\mu}} W + O(v^4),\end{aligned}\tag{100}$$

where

$$W = \frac{\mathbf{e}_\pm \cdot \mathbf{r}}{r} \left[ R(r) + \frac{3}{4m_c^2} R''(r) + O(v^4) \right],\tag{101}$$

and  $R(r)$  is the radial part of the P-wave charmonium in its rest frame (see derivation in Appendix A of [2]). The new notations for the polarization vectors



are,

$$\begin{aligned} e_+ &= -\frac{e_x + ie_y}{\sqrt{2}}, \\ e_- &= \frac{e_x - ie_y}{\sqrt{2}}. \end{aligned} \quad (102)$$

In what follows we use the LC wave functions of gluons and charmonium in order to calculate matrix elements of operators which depend only on the LC variables  $r$  and  $\alpha$ . Therefore, for the sake of simplicity we can drop off the indexes  $\mu, \bar{\mu}$  and summation over them, *i.e.* replace

$$\sum_{\mu\bar{\mu}} \left( \Phi_\chi^{\mu\bar{\mu}}(\mathbf{r}, \alpha) \right)^* \Phi_G^{\mu\bar{\mu}}(\mathbf{r}, \alpha) \Rightarrow \Phi_\chi^*(\mathbf{r}, \alpha) \Phi_G(\mathbf{r}, \alpha) \quad (103)$$

With this convention we can rewrite the cross section Eq. (92) as,

$$\begin{aligned} \sigma(GN \rightarrow \chi X) &= \int_0^1 d\alpha \int_0^1 d\alpha' \int d^2r d^2r' \\ &\times \left\{ \Phi_\chi^*(\mathbf{r}, \alpha) \Phi_\chi(\mathbf{r}', \alpha') \Sigma^{tr}(\mathbf{r}, \mathbf{r}', \alpha, \alpha') \Phi_G(\mathbf{r}, \alpha) \Phi_G^*(\mathbf{r}', \alpha') \right\}, \end{aligned} \quad (104)$$

where the transition cross section  $\Sigma^{tr}$  is a combination of dipole cross sections,

$$\Sigma^{tr}(\mathbf{r}, \mathbf{r}', \alpha, \alpha') = \frac{1}{16} \left[ \sigma_{\bar{q}q}(\mathbf{r}_1 - \mathbf{r}'_2) + \sigma_{q\bar{q}}(\mathbf{r}_2 - \mathbf{r}'_1) - \sigma_{q\bar{q}}(\mathbf{r}_1 - \mathbf{r}'_1) - \sigma_{\bar{q}q}(\mathbf{r}_2 - \mathbf{r}'_2) \right], \quad (105)$$

and  $\mathbf{r}_1, \mathbf{r}'_2, \mathbf{r}'_1$  and  $\mathbf{r}_2$  are defined like in Eq. (93).

## 9 Charmonium hadroproduction off nuclei

Nuclear effects in charmonium production have drawn much attention during the last two decades since the NA3 experiment at CERN [92] has found a steep increase of nuclear suppression with rising Feynman  $x_F$ . This effect has been confirmed later in the same energy range [93], and at higher energy recently by the most precise experiment E866 at Fermilab [94]. No unambiguous explanation for these observations has been provided yet. With the advent of RHIC new data are expected soon in the unexplored energy range. Lacking a satisfactory understanding of nuclear effects for charmonium production in proton-nucleus collisions it is very difficult to provide a convincing interpretation of data from heavy ion collisions experiments [95,96] which are aimed to detect the creation of a quark-gluon plasma using charmonium as a sensitive probe. Many of existing analyses rely on an oversimplified dynamics of charmonium production which fail to explain even data for  $pA$  collisions, in particular the observed  $x_F$  dependence of  $J/\Psi$  suppression. Moreover, sometimes even predictions for RHIC employ those simple models. It is our purpose to demonstrate that the dynamics of

charmonium suppression strikingly changes between the SPS and RHIC energies. We perform full QCD calculations of nuclear effects within the framework of the light-cone Green function approach aiming to explain observed nuclear effects without adjusting any parameters, and to provide realistic predictions for RHIC.

To avoid a confusion, we should make it clear that we will skip discussion of any mechanisms of charmonium suppression caused by the interaction with the produced comoving matter, although it should be an important effect in central heavy ion collisions. Instead, we consider suppression which originates from the production process and propagation of the  $c\bar{c}$  pair through the nucleus. It serves as a baseline for search for new physics in heavy ion collisions.

We focus here on coherence phenomena which are still a rather small correction for charmonium production at the SPS, but whose onset has already been observed at Fermilab and which are expected to become a dominant effect at the energies of RHIC and LHC. One realizes the importance of the coherence effects treating charmonium production in an intuitive way as a hard  $c\bar{c}$  fluctuation that loses coherence with the projectile ensemble of partons via interaction with the target, and is thus liberated. In spite of the hardness of the fluctuation, its lifetime in the target rest frame increases with energy and eventually exceeds the nucleus size. Apparently, in this case the  $c\bar{c}$  pair is freed by interaction with the whole nucleus, rather than with an individual bound nucleon as it happens at low energies. Correspondingly, nuclear effects become stronger at high energies since the fluctuation propagates through the whole nucleus, and different nucleons compete with each other in freeing the  $c\bar{c}$ . In terms of the conventional Glauber approach it leads to shadowing. In terms of the parton model it is analogous to shadowing of  $c$ -quarks in the nuclear structure function. It turns out (see Sect. 9.3) that the fluctuations containing gluons in addition to the  $c\bar{c}$  pair are subject to especially strong shadowing. Since at high energies the weight of such fluctuations rises, as well as the fluctuation lifetime, it becomes the main source of nuclear suppression of open and hidden charm at high energies, in particular at RHIC. In terms of the parton model, shadowing for such fluctuations containing gluons correspond to gluon shadowing.

The parton model interpretation of charmonium production contains no explicit coherence effects, but they are hidden in the gluon distribution function of the nucleus which is supposed to be subject to QCD factorization. There are, however, a few pitfalls on this way. First of all, factorization is exact only in the limit of a very hard scale. That means that one should neglect the effects of the order of the inverse  $c$ -quark mass, in particular the transverse  $c\bar{c}$  separation  $\langle r^2 \rangle \sim 1/m_c^2$ . However, shadowing and absorption of  $c\bar{c}$  fluctuations is a source of a strong suppression which is nearly factor of 0.5 for heavy nuclei (see Fig. 18). QCD factorization misses this effect. Second of all, according to factorization gluon shadowing is supposed to be universal, *i.e.* one can borrow it from another process (although we still have no experimental information about gluon shadowing, it only can be calculated) and use to predict nuclear suppression of open or hidden charm. Again, factorization turns out to be dramatically violated at the scale of charm and gluon shadowing for charmonium production is much

stronger than it is for open charm or deep-inelastic scattering (DIS) (compare gluon shadowing exposed in Fig. 21 with one calculated in Ref. [29] for DIS). All these important, sometimes dominant effects are missed by QCD factorization. This fact once again emphasizes the advantage of the light-cone dipole approach which does reproduce QCD factorization in the limit where it is expected to work, and which is also able to calculate the deviations from factorization in a parameter free way.

Unfortunately, none of the existing models for  $J/\Psi$  or  $\Psi'$  production in  $NN$  collisions is fully successful in describing all the features observed experimentally. In particular, the  $J/\Psi$ ,  $\Psi'$  and  $\chi_1$  production cross sections in  $NN$  collisions come out too small by at least an order of magnitude [97]. Only data for production of  $\chi_2$  whose mechanism is rather simple seems to be in good accord with the theoretical expectation based on the color singlet mechanism (CSM) [98,99] treating  $\chi_2$  production via glue-gluon fusion. The contribution of the color-octet mechanism is an order of magnitude less than that of CSM [99], and is even more suppressed according to Ref. [100]. The simplicity of the production mechanism of  $\chi_2$  suggests to use this process as a basis for the study of nuclear effects. Besides, about 40% of the  $J/\Psi$ s have their origin in  $\chi$  decays. We drop the subscript of  $\chi_2$  in what follows unless otherwise specified.

### 9.1 Interplay of formation and coherence time scales and related phenomena

A lot of work has been done and considerable progress has been achieved in the understanding of many phenomena related to the dynamics of the charmonium production and nuclear suppression.

- Relative nuclear suppression of  $J/\Psi$  and  $\Psi'$  has attracted much attention. The  $\Psi'$  has twice as large a radius as the  $J/\Psi$ , therefore should attenuate in nuclear matter much stronger. However, formation of the wave function of the charmonia takes time, one cannot instantaneously distinguish between these two levels. This time interval or so called formation time (length) is enlarged at high energy  $E_\Psi$  by Lorentz time dilation,

$$t_f = \frac{2 E_\Psi}{M_{\Psi'}^2 - M_{J/\Psi}^2}, \quad (106)$$

and may become comparable to or even longer than the nuclear radius. In this case neither  $J/\Psi$ , nor  $\Psi'$  propagates through the nuclear medium, but a preformed  $c\bar{c}$  wave packet [23]. Intuitively, one might even expect a universal nuclear suppression, indeed supported by data [77,95,94]. However, a deeper insight shows that such a point of view is oversimplified, namely, the mean transverse size of the  $c\bar{c}$  wave packet propagating through the nucleus varies depending on the wave function of the final meson on which the  $c\bar{c}$  is projected. In particular, the nodal structure of the  $2S$  state substantially enhances the yield of  $\Psi'$  [33,39] (see in [101,102] a complementary interpretation in the hadronic basis).

- The next phenomenon is related to the so called coherence time. Production of a heavy  $c\bar{c}$  is associated with a longitudinal momentum transfer  $q_c$  which

decreases with energy. Therefore the production amplitudes on different nucleons add up coherently and interfere if the production points are within the interval  $l_c = 1/q_c$  called coherence length or time,

$$t_c = \frac{2 E_\Psi}{M_{J/\Psi}^2}. \quad (107)$$

This time interval is much shorter than the formation time Eq. (106). One can also interpret it in terms of the uncertainty principle as the mean lifetime of a  $c\bar{c}$  fluctuation. If the coherence time is long compared to the nuclear radius,  $t_c \gtrsim R_A$ , different nucleons compete with each other in producing the charmonium. Therefore, the amplitudes interfere destructively leading to an additional suppression called shadowing. Predicted in Ref. [33], this effect was confirmed by the NMC measurements of exclusive  $J/\Psi$  photoproduction off nuclei [76] (see also Ref. [39]). The recent precise data from the HERMES experiment [103] for electroproduction of  $\rho$  mesons also confirms the strong effect of coherence time [104].

Note that the coherence time Eq. (107) is relevant only for the lightest fluctuations  $|c\bar{c}\rangle$ . Heavier ones which contain additional gluons have shorter lifetime. However, at high energies they are also at work and become an important source of an extra suppression (see Ref. [29] and Sect. 9.3). They correspond to shadowing of gluons in terms of parton model. In terms of the dual parton model the higher Fock states contain additional  $q\bar{q}$  pairs instead of gluons. Their contribution is enhanced on a nuclear target and leads to softening of the  $x_F$  distribution of the produced charmonium. This mechanism has been used in Ref. [105] to explain the  $x_F$  dependence of charmonium suppression. However the approach was phenomenological and data were fitted.

The first attempt to implement the coherence time effects into the dynamics of charmonium production off nuclei has been made in Ref. [106]. However, the approach still was phenomenological and data also were fitted. Besides, gluon shadowing (see Sect. 9.3) had been missed.

- The total  $J/\Psi$ -nucleon cross section steeply rises with energy, approximately as  $s^{0.2}$ . This behavior is suggested by the observation of a steep energy dependence of the cross section of  $J/\Psi$  photoproduction at HERA. This fact goes well along with observation of the strong correlation between  $x_{Bj}$  dependence of the proton structure function at small  $x_{Bj}$  and the photon virtuality  $Q^2$ : the larger is  $Q^2$  (the smaller is its  $q\bar{q}$  fluctuation), the steeper the rises  $F_2(x_{Bj}, Q^2)$  with  $1/x_{Bj}$ . Apparently, the cross section of a small size charmonium must rise with energy faster than what is known for light hadrons. The  $J/\Psi$ -nucleon cross section has been calculated recently in Ref. [1] employing the light-cone dipole phenomenology, realistic charmonium wave functions and phenomenological dipole cross section fitted to data for  $F_2(x, Q^2)$  from HERA. The results are in a good accord with data for the electroproduction cross sections of  $J/\Psi$  and  $\Psi'$  and also confirm the steep energy dependence of the charmonium-nucleon cross sections (see sect. 4). Knowledge of these cross sections is very important for the understanding of nuclear effects in the production of char-

monia. A new important observation made in Ref. [1] is a strong effect of spin rotation associated with boosting the  $c\bar{c}$  system from its rest frame to the light cone. It substantially increases the  $J/\Psi$  and especially  $\Psi'$  photoproduction cross sections. The effect of spin rotation is also implemented in our calculations below and it is crucial for restoration of the Landau-Yang theorem [2,91].

- Initial state energy loss by partons traveling through the nucleus affects the  $x_F$  distribution of produced charmonia [107] especially at medium high energies. A shift in the effective value of  $x_1$ , which is the fraction of the incident momentum carried by the produced charmonium, and the steep  $x_1$ -dependence of the cross section of charmonium production off a nucleon lead to a dramatic nuclear suppression at large  $x_1$  (or  $x_F$ ) in a good agreement with data [92,93]. The recent analyses [90] of data from the E772 experiment for Drell-Yan process on nuclei reveals for the first time a nonzero and rather large energy loss.

## 9.2 Higher twist nuclear effects

Nuclear effects in the production of a  $\chi$  are controlled by the coherence and formation lengths which are defined in Eqs. (106), (107). One can identify two limiting cases. The first one corresponds to the situation where both  $l_c$  and  $l_f$  are shorter than the mean spacing between bound nucleons. In this case one can treat the process classically, the charmonium is produced on one nucleon inside the nucleus and attenuates exponentially with an absorptive cross section which is the inelastic  $\chi - N$  one. This simplest case is described in Refs. [107,11].

In the limit of a very long coherence length  $l_c \gg R_A$  one can think about a  $c\bar{c}$  fluctuation which emerges inside the incident hadron long before the interaction with the nucleus. Different bound nucleons compete and shadow each other in the process of liberation of this fluctuation. This causes an additional attenuation in addition to inelastic collisions of the produced color-singlet  $c\bar{c}$  pair on its way out of the nucleus. Since  $l_c \ll l_f$  an intermediate case is also possible where  $l_c$  is shorter than the mean internucleon separation, while  $l_f$  is of the order or longer than the nuclear radius.

The transition between the limits of very short and very long coherence lengths is performed using the prescription suggested in Ref. [51] for inelastic photoproduction of  $J/\Psi$  off nuclei. The amplitude of  $\chi$  production off a nucleus can be represented in the form,

$$A^{(\lambda)}(b, z) = \int_0^1 d\alpha \int d^2r \int d^2r' \Phi_\chi^*(\mathbf{r}, \alpha) \hat{D}^{(\lambda)}(\mathbf{r}, \mathbf{r}', \alpha; b, z) \Phi_G(\mathbf{r}', \alpha), \quad (108)$$

where  $\hat{D}^{(\lambda)}(\mathbf{r}, \mathbf{r}', \alpha; b, z)$  is the amplitude of production of a colorless  $c\bar{c}$  pair which reaches a separation  $\mathbf{r}$  outside the nucleus. It is produced at the point  $(\mathbf{b}, z)$  by a color-octet  $c\bar{c}$  with separation  $r'$ . The amplitude consists of two terms,

$$\hat{D}^{(\lambda)}(\mathbf{r}, \mathbf{r}', \alpha; b, z) = \hat{D}_1^{(\lambda)}(\mathbf{r}, \mathbf{r}', \alpha; b, z) + \hat{D}_2^{(\lambda)}(\mathbf{r}, \mathbf{r}', \alpha; b, z). \quad (109)$$

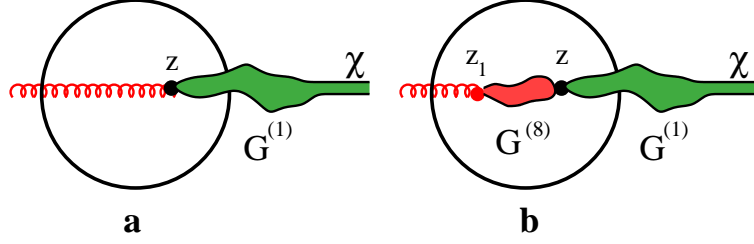


**Fig. 17.** The incident gluon can either produce the colorless  $c\bar{c}$  pair with quantum numbers of  $\chi$  at the point  $z$  (**a**), or it produces diffractively a color-octet  $c\bar{c}$  with the quantum numbers of the gluon at the point  $z_1$  which is then converted into a color singlet state at  $z$  (**b**). Propagation of a color-singlet or octet  $c\bar{c}$  is described by the Green functions  $G_{c\bar{c}}^{(1)}$  and  $G_{c\bar{c}}^{(8)}$ , respectively.

Here the first term reads,

$$\hat{D}_1^{(\lambda)}(\mathbf{r}, \mathbf{r}', \alpha; b, z) = G_{c\bar{c}}^{(1)}(\mathbf{r}, z_+; \mathbf{r}', z) e^{(\lambda)} \cdot \mathbf{d}' e^{iq_L z}, \quad (110)$$

where  $G_{c\bar{c}}^{(1)}(\mathbf{r}, z_+; \mathbf{r}', z)$  is the color-singlet Green function describing evolution of a  $c\bar{c}$  wave packet with initial separation  $\mathbf{r}'$  at the point  $z$  up to the final separation  $\mathbf{r}$  at  $z_+ \rightarrow \infty$ . This term is illustrated in Fig. 17a.

There is also a possibility for the projectile gluon to experience diffractive interaction with production of color-octet  $c\bar{c}$  with the same quantum numbers of the gluon at the point  $z_1$ . This pair propagates from the point  $z_1$  to  $z$  as is described by the corresponding color-octet Green function  $G_{c\bar{c}}^{(8)}$  and produces the final colorless pair which propagation is described by the color-singlet Green function, as is illustrated in Fig. 17b. The corresponding second term in Eq. (109) reads,

$$\begin{aligned} \hat{D}_2^{(\lambda)}(\mathbf{r}, \mathbf{r}', \alpha; b, z) = & -\frac{1}{2} \int_{-\infty}^z dz_1 d^2 r'' G_{c\bar{c}}^{(1)}(\mathbf{r}, z_+; \mathbf{r}'', z) \\ & \times e^{(\lambda)} \cdot \mathbf{d}'' G_{c\bar{c}}^{(8)}(\mathbf{r}'', z; \mathbf{r}', z_1) e^{iq_L z_1} \sigma_{q\bar{q}G}(\mathbf{r}', \alpha) \rho_A(b, z_1). \end{aligned} \quad (111)$$

The singlet,  $G_{c\bar{c}}^{(1)}$ , and octet,  $G_{c\bar{c}}^{(8)}$ , Green functions describe the propagation of color-singlet and octet  $c\bar{c}$ , respectively, in the nuclear medium. They satisfy the Schrödinger equations,

$$i \frac{d}{dz} G_{c\bar{c}}^{(k)}(\mathbf{r}, \mathbf{r}'; z, z') = \left[ \frac{m_c^2 - \Delta_{\mathbf{r}}}{2E_G \alpha (1 - \alpha)} + V^{(k)}(\mathbf{r}, \alpha) \right] G_{c\bar{c}}^{(k)}(\mathbf{r}, \mathbf{r}'; z, z'), \quad (112)$$

with  $k = 1, 8$  and boundary conditions

$$G_{c\bar{c}}^{(k)}(\mathbf{r}, \mathbf{r}'; z, z') \Big|_{z=z'} = \delta(\mathbf{r} - \mathbf{r}'). \quad (113)$$

The imaginary part of the LC potential  $V^{(k)}$  is responsible for the attenuation in nuclear matter,

$$\text{Im } V^{(k)}(\mathbf{r}, \alpha) = -\frac{1}{2} \sigma^{(k)}(r, \alpha) \rho_A(b, z) , \quad (114)$$

where

$$\begin{aligned} \sigma^{(1)}(r, \alpha) &= \sigma_{q\bar{q}}(r) , \\ \sigma^{(8)}(r, \alpha) &= \sigma_3(r, \alpha) . \end{aligned} \quad (115)$$

The real part of the LC potential  $V^{(k)}(\mathbf{r}, \alpha)$  describes the interaction inside the  $c\bar{c}$  system. For the singlet state  $\text{Re } V^{(1)}(\mathbf{r}, \alpha)$  should be chosen to reproduce the charmonium mass spectrum. With a realistic potential (see *e.g.* Ref. [1]) one can solve Eq. (112) only numerically. Since we focus here on the principle problems of understanding of the dynamics of nuclear shadowing in charmonium production, we chose the oscillator form of the potential [29],

$$\text{Re } V^{(1)}(\mathbf{r}, \alpha) = \frac{a^4(\alpha) r^2}{2 E_G \alpha (1 - \alpha)} , \quad (116)$$

where

$$\begin{aligned} a(\alpha) &= 2 \sqrt{\alpha(1 - \alpha)} \mu \omega , \\ \mu &= \frac{m_c}{2} , \quad \omega = 0.3 \text{ GeV} . \end{aligned} \quad (117)$$

The LC potential Eq. (116) corresponds to a choice of a potential,

$$U(\mathbf{R}) = \frac{1}{2} \mu \omega \mathbf{R}^2 , \quad (118)$$

in the nonrelativistic Schrödinger equation,

$$\left[ -\frac{\Delta}{2\mu} + U(\mathbf{R}) \right] \Psi(\mathbf{R}) = E \Psi(\mathbf{r}) , \quad (119)$$

which should describe the bound states of a colorless  $c\bar{c}$  system. Of course this is an approximation we are forced to do in order to solve the evolution equation analytically.

To describe color-octet  $c\bar{c}$  pairs we fix the corresponding potential at

$$\text{Re } V^{(8)}(\mathbf{r}, \alpha) = 0 , \quad (120)$$

in order to reproduce the gluon wave function Eq. (95).

To keep calculations simple we use the  $r^2$ -approximation Eq. (17) for the dipole cross section which is reasonable for small-size heavy quark systems. Then, taking into account Eqs. (114) - (116) we arrive at the final expressions,

$$V^{(k)}(r, \alpha) = \frac{1}{2} \kappa^{(k)} r^2 , \quad (121)$$

$$\kappa^{(1)} = \frac{a^4(\alpha)}{\alpha(1-\alpha)E_G} - iC(s)\rho_A, \quad (122)$$

$$\kappa^{(8)} = -iC(s)\rho_A \left\{ \frac{9}{8} [\alpha^2 + (1-\alpha)^2] - \frac{1}{8} \right\}. \quad (123)$$

Making use of this approximation and assuming a constant nuclear density  $\rho_A(b, z) = \rho_A$  the Green functions can be obtained in an analytical form,

$$G_{c\bar{c}}^{(k)}(\mathbf{r}, \mathbf{r}'; z_2, z_1) = \frac{b^{(k)}}{2\pi \sinh(\Omega^{(k)} \Delta z)} \times \exp \left\{ -\frac{b^{(k)}}{2} \left[ \frac{\mathbf{r}^2 + \mathbf{r}'^2}{\tanh(\Omega^{(k)} \Delta z)} - \frac{2\mathbf{r} \cdot \mathbf{r}'}{\sinh(\Omega^{(k)} \Delta z)} \right] \right\} \quad (124)$$

where

$$\begin{aligned} b^{(k)} &= \sqrt{\kappa^{(k)} E_G \alpha(1-\alpha)}, \\ \Omega^{(k)} &= \frac{b^{(k)}}{E_G \alpha(1-\alpha)}, \\ \Delta z &= z_2 - z_1. \end{aligned}$$

We define the nuclear transparency for  $\chi$  production as

$$Tr_A(\chi) = \frac{\sigma(GA \rightarrow \chi X)}{A\sigma(GN \rightarrow \chi X)}. \quad (125)$$

It depends only on the  $\chi$  or projectile gluon energy. We plot our predictions for lead in Fig. 18.

Transparency rises at low energy since the formation length increases and the effective absorption cross section becomes smaller. This behavior, assuming  $l_c = 0$ , is shown by dashed curve. However, at higher energies the coherence length is switched on and shadowing adds to absorption. As a result, transparency decreases, as is shown by the solid curve. On top of that, the energy dependence of the dipole cross section makes those both curves for  $Tr_A(E_\chi)$  fall even faster.

Apparently, the nuclear transparency depends only on the  $\chi$  energy, rather than the incident energy or  $x_1$ . It is interesting that this leads to  $x_2$  scaling. Indeed, the  $\chi$  energy

$$E_\chi = \frac{M_\chi^2}{2m_N x_2}, \quad (126)$$

depends only on  $x_2$ . We show the  $x_2$  scale in Fig. 18 (top) along with energy dependence.

We also compare in Fig. 19 the contribution of quark shadowing and absorption (thin solid curve) with the nuclear suppression observed at 800 GeV [94]. Since data are for  $W/Be$  ratio, and our constant density approximation should not be applied to beryllium, we assume for simplicity that all  $pA$  cross sections including  $pN$  obey the  $A^{\alpha(x_F)}$ . We see that the calculated contribution has quite a different shape from what is suggested by the data. It also leaves plenty of room for complementary mechanisms of suppression at large  $x_F$  (see below).



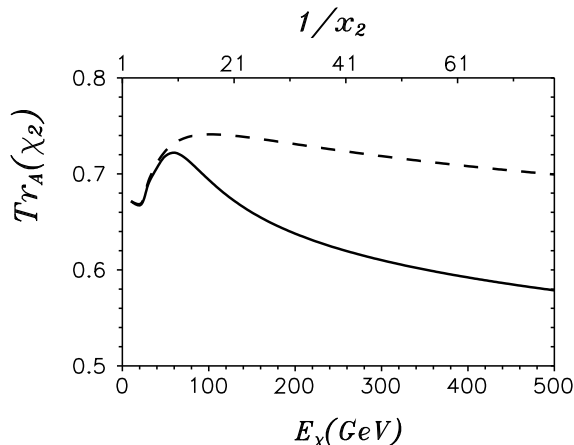


**Fig. 18.** Nuclear transparency for  $\chi$  production off lead as function of energy of the charmonium, or  $x_2$  (the upper scale). The solid curve includes both effects of coherence and formation, while the dashed curve corresponds to  $l_c = 0$ . Since transparency scales in  $x_2$  according to (126), values of  $x_2$  are shown on the top axis.

### 9.3 Leading twist gluon shadowing

Previously we considered only the lowest  $|c\bar{c}\rangle$  fluctuation of the gluon, which is apparently an approximation. The higher Fock components containing gluons should be also included. In fact they are already incorporated in the phenomenological dipole cross section we use, and give rise to the energy dependence of  $\sigma_{q\bar{q}}$ . However, they are still excluded from nuclear effects. Indeed, although we eikonalize the energy dependent dipole cross section the higher Fock components do not participate in that procedure, but they have to be eikonalized as well. This corrections, as is demonstrated below, correspond to suppression of gluon density in nuclei at small  $x$ .

The gluon density at small  $x$  in nuclei is known to be shadowed, *i.e.* reduced compared to a free nucleons. The partonic interpretation of this phenomenon looks very different depending on the reference frame. In the infinite momentum frame, as was first suggested by Kancheli [108], the partonic clouds of nucleons are squeezed by the Lorentz transformation less at small than at large  $x$ . Therefore, while these clouds are well separated in longitudinal direction at large  $x$ , they overlap and can fuse at small  $x$ , resulting in a diminished parton density [108,9].

Different observables can probe this effect. Nuclear shadowing of the DIS inclusive cross section or Drell-Yan process demonstrate a reduction of the sea quark density at small  $x$ . Charmonium or open charm production is usually considered as a probe for gluon distribution.

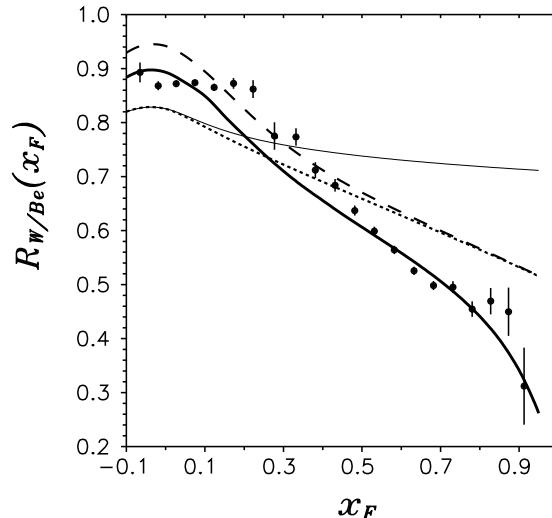


**Fig. 19.** Tungsten to beryllium cross section ratio as function of Feynman  $x_F$  for  $J/\Psi$  production at proton energy 800 GeV. The thin solid curve represents contribution of initial state quark shadowing and final state  $c\bar{c}$  attenuation for  $\chi$  production. The dotted curve includes also gluon shadowing. The dashed curve is corrected for gluon enhancement at large  $x_2$  (small  $x_F$ ) using the prescription from [78]. The final solid curve is also corrected for energy loss and for  $\chi \rightarrow J/\Psi\gamma$  decay. Experimental points are from the E866 experiment [94].

Although observables are Lorentz invariant, partonic interpretations are not, and the mechanism of shadowing looks quite different in the rest frame of the nucleus where it should be treated as Gribov's inelastic shadowing. This approach seems to go better along with our intuition, besides, the interference or coherence length effects governing shadowing are under a better control. One can even calculate shadowing in this reference frame in a parameter free way (see Refs. [58,83,29]) employing the well developed phenomenology of color dipole representation suggested in Ref. [13]. On the other hand, within the parton model one can only calculate the  $Q^2$  evolution of shadowing which is quite a weak effect. The main contribution to shadowing originates from the fitted to data input.

In the color dipole representation nuclear shadowing can be calculated via simple eikonalization of the elastic amplitude for each Fock component of the projectile light-cone wave function which are the eigenstates of interaction [13]. Different Fock components represent shadowing of different species of partons. The  $|q\bar{q}\rangle$  component in DIS or  $|q\gamma^*\rangle$  in Drell-Yan reaction should be used to calculate shadowing of sea quarks. The same components including also one or more gluons lead to gluon shadowing [88,29].

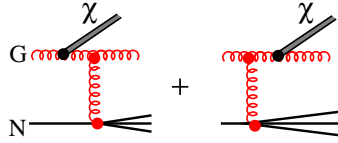


**Fig. 20.** The dominant Feynman diagrams contributing to  $\chi$  production.

In the color dipole approach one can explicitly see deviations from QCD factorization, *i.e.* dependence of the measured parton distribution on the process measuring it. For example, the coherence length and nuclear shadowing in the Drell-Yan process vanish at minimal  $x_2$  (at fixed energy) [90], while the factorization predicts maximal shadowing. Here we present even more striking deviation from factorization, namely, gluon shadowing for charmonium production turns out to be dramatically enhanced compared to DIS.

#### 9.4 LC dipole representation for the reaction $GN \rightarrow \chi GX$

In the case of charmonium production, different Fock components of the projectile gluon,  $|(c\bar{c})_1 nG\rangle$  containing a colorless  $c\bar{c}$  pair and  $n$  gluons ( $n = 0, 1 \dots$ ) build up the cross section of charmonium production which steeply rises with energy (see Ref. [1]). The cross section is expected to factorize in impact parameter representation in analogy to the DIS and Drell Yan reaction. This representation has the essential advantage in that nuclear effects can be easily calculated [15,83]. Feynman diagrams corresponding  $\chi$  production associated with gluon radiation are shown in Appendix D of [2]. We treat the interaction of heavy quarks perturbatively in the lowest order approximation, while the interaction with the nucleon is soft and expressed in terms of the gluon distribution. The calculations are substantially simplified if the radiated gluon takes a vanishing fraction  $\alpha_3$  of the total light-cone momentum and the heavy quarkonium can be treated as a nonrelativistic system. In this case the amplitude of  $\chi G$  production has a simple form that corresponds to the ‘‘Drell-Yan’’ mechanism of  $\chi$  production illustrated in Fig. 20.

Correspondingly, the cross section of  $\chi$  production has the familiar factorized form similar to the Drell-Yan reaction [15,82,83],

$$\alpha_3 \frac{d\sigma(GN \rightarrow \chi GX)}{d\alpha_3} = \int d^2s |\Psi_{G\chi}(s, \alpha_3)|^2 \sigma_{GG}[(1 - \alpha_3)\mathbf{s}, x_2/\alpha_3] , \quad (127)$$

where  $\sigma_{GG}(r, x) = 9/4 \sigma_{q\bar{q}}(r, x)$  is the cross section of interaction of a  $GG$  dipole with a nucleon.  $\Psi(s, \alpha_3)$  is the effective distribution amplitude for the  $\chi - G$  fluctuation of a gluon, which is the analog to the  $\gamma^* q$  fluctuation of a quark,

$$\begin{aligned} \Psi_{G\chi}(s, \alpha_3) &= \sum_{\bar{\mu}\mu} \int d^2r d\alpha \Phi_{\chi}^{\bar{\mu}\mu}(\mathbf{r}, \alpha) \Phi_G^{\bar{\mu}\mu}(\mathbf{r}, \alpha) \\ &\times \left[ \Phi_{cG}\left(\mathbf{s} + \frac{\mathbf{r}}{2}, \frac{\alpha_3}{\alpha}\right) - \Phi_{cG}\left(\mathbf{s} - \frac{\mathbf{r}}{2}, \frac{\alpha_3}{1 - \alpha}\right) \right] . \end{aligned} \quad (128)$$

Here,  $\Phi_\chi^{\bar{\mu}\mu}(\mathbf{r}, \alpha)$  and  $\Phi_G^{\bar{\mu}\mu}(\mathbf{r}, \alpha)$  are the  $q\bar{q}$  LC wave functions of the  $\chi$  and gluon, respectively, which depend on transverse separation  $\mathbf{r}$  and relative sharing  $\alpha$  by the  $q\bar{q}$  of the total LC momentum.  $\Phi_{cG}(\mathbf{s}, \alpha)$  is the LC wave function of a quark-gluon Fock component of a quark.

### 9.5 Gluon shadowing for $\chi$ production off nuclei

The gluon density in nuclei is known to be modified, shadowed at small Bjorken  $x$ . Correspondingly, production of  $\chi$  treated as gluon-gluon fusion must be additionally suppressed. In the rest frame of the nucleus, gluon shadowing appears as Gribov's inelastic shadowing [57], which is related to diffractive gluon radiation. The rest frame seems to be more convenient to calculate gluon shadowing, since techniques are better developed, and we use it in what follows. The process  $GN \rightarrow \chi X$  considered in the previous section includes by default radiation of any number of gluons which give rise to the energy dependence of the dipole cross section.

Extending the analogy between the reactions of  $\chi G$  production by an incident gluon and heavy photon radiation by a quark to the case of nuclear target one can write an expression for the cross section of reaction  $GA \rightarrow \chi GX$  in two limiting cases:

(i) the production occurs nearly instantaneously over a longitudinal distance which is much shorter than the mean free path of the  $\chi G$  pair in nuclear matter. In this case the cross sections on a nuclear and nucleon targets differ by a factor  $A$  independently of the dynamics of  $\chi G$  production.

(ii) The lifetime of the  $\chi G$  fluctuation,

$$t_c = \frac{2 E_G}{M_{\chi G}^2}, \quad (129)$$

substantially exceeds the nuclear size. It is straightforward to replace the dipole cross section on a nucleon by a nuclear one [15,83], then Eq. (127) is modified to

$$\frac{d\sigma(GA \rightarrow \chi GX)}{d(\ln \alpha_3)} = 2 \int d^2b d^2s |\Psi_{G\chi}(\mathbf{s}, \alpha_3)|^2 \times \left\{ 1 - \exp \left[ -\frac{1}{2} \sigma_{GG}(\mathbf{s}, x_2/\alpha_3) T_A(b) \right] \right\}. \quad (130)$$

In order to single out the net gluon shadowing we exclude here the size of the  $c\bar{c}$  pair assuming that the cross section responsible for shadowing depends only on the transverse separation  $\mathbf{s}$ .

(iii) A general solution valid for any value of  $t_c$  is more complicated and must interpolate between the above limiting situations. In this case one can use the methods of the Landau-Pomeranchuk-Migdal (LPM) theory for photon bremsstrahlung in a medium generalized for targets of finite thickness in [109,83]. The general expressions for the cross section which reproduces the limiting cases

$t_c \rightarrow 0$  (i) and  $t_c \rightarrow \infty$  (ii) reads,

$$\begin{aligned} \frac{d\sigma(GA \rightarrow \chi GX)}{d^2bd \ln \alpha_3} &= \left\{ \int_{-\infty}^{\infty} dz \rho_A(b, z) \right. \\ &\times \int d^2s |\Psi_{G\chi}(s, \alpha_3)|^2 \sigma_{GG} [(1 - \alpha_3)\mathbf{s}, x_2/\alpha_3] \\ &\left. - \frac{1}{2} \text{Re} \int_{-\infty}^{\infty} dz_2 \rho_A(b, z_2) \int_{-\infty}^{z_2} dz_1 \rho_A(b, z_1) \tilde{\Sigma}(z_2, z_1) e^{iqL(z_2 - z_1)} \right\}, \quad (131) \end{aligned}$$

where

$$\begin{aligned} \tilde{\Sigma}(z_2, z_1) &= \int d^2s_1 d^2s_2 \Psi_{G\chi}^*(\mathbf{s}_2, \alpha_3) \sigma_{GG}(s_2, x_2/\alpha_3) G(\mathbf{s}_2, z_2; \mathbf{s}_1, z_1) \\ &\times \sigma_{GG}(s_1, x_2/\alpha_3) \Psi_{G\chi}(\mathbf{s}_1, \alpha_3). \quad (132) \end{aligned}$$

To single out the correction for gluon shadowing one should compare the cross section Eq. (131) with the impulse approximation term in which absorption is suppressed,

$$R_G(x_2) = \frac{G_A(x_2)}{A G_N(x_2)} = 1 - \frac{1}{A \sigma(GN \rightarrow \chi X)} \int_{x_2}^{\alpha_{max}} d\alpha_3 \frac{d\sigma(GA \rightarrow \chi GX)}{d\alpha_3}. \quad (133)$$

For further calculations and many other applications one needs to know gluon shadowing as function of impact parameter which is calculated as follows,

$$\begin{aligned} R_G(x_2, b) &= \frac{G_A(x_2, b)}{T_A(b) G_N(x_2)} \\ &= 1 - \frac{1}{T_A(b) \sigma(GN \rightarrow \chi X)} \int_{x_2}^{\alpha_{max}} d\alpha_3 \frac{d\sigma(GA \rightarrow \chi GX)}{d^2b d\alpha_3}. \quad (134) \end{aligned}$$

The results of calculations for the  $b$ -dependence of gluon shadowing (134) are depicted in Fig. 21 for different values of  $x_2$  as function of thickness of nuclear matter,  $L = \sqrt{R_A^2 - b^2}$ .

The results confirm the obvious expectation that shadowing increases for smaller  $x_2$  and for longer path in nuclear matter. One can see that for given thickness shadowing tends to saturate down to small  $x_2$ , what might be a result of one gluon approximation. Higher Fock components with larger number of gluons are switched on at very small  $x_2$ . At the same time, shadowing saturates at large lengths what one should have also expected as a manifestation of gluon saturation. Note that at large  $x_2 = 0.03$  shadowing is even getting weaker at longer  $L$ . This is easy to understand, in the case of weak shadowing one can drop off the multiple scattering terms higher than two-fold one. Then the shadowing correction is controlled by the longitudinal formfactor of the nucleus which decreases with  $L$  (it is obvious for the Gaussian shape of the nuclear density, but is also true for the realistic Woods-Saxon distribution).

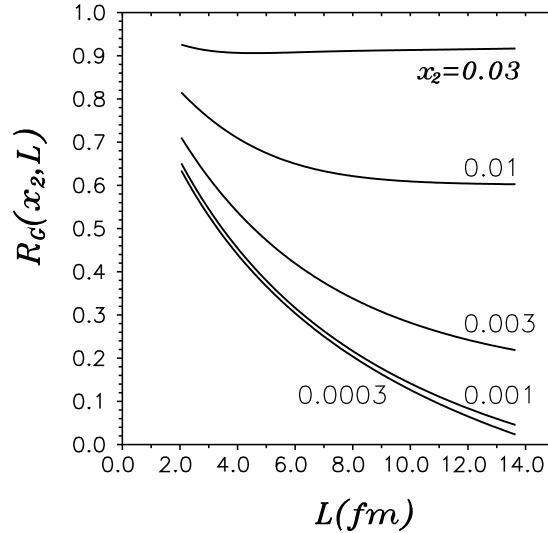


**Fig. 21.** Gluon suppression as function of thickness of nuclear matter with constant density  $\rho_A = 0.16 \text{ fm}^{-3}$ .

### 9.6 Antishadowing of gluons

Nuclear modification of the gluon distribution is poorly known. There is still no experimental evidence for that. Nevertheless, the expectation of gluon shadowing at small  $x$  is very solid, and only its amount might be disputable. At the same time, some indications exist that gluons may be enhanced in nuclei at medium small  $x_2 \sim 0.1$ . The magnitude of gluon antishadowing has been estimated in Ref. [45] assuming that the total fraction of momentum carried by gluons is the same in nuclei and free nucleons (there is an experimental support for it). Such a momentum conservation sum rule leads to a gluon enhancement at medium  $x$ , since gluons are suppressed in nuclei at small  $x$ . The effect, up to  $\sim 20\%$  antishadowing in heavy nuclei at  $x \approx 0.1$ , found in Ref. [45] is rather large, but it is a result of very strong shadowing which we believe has been grossly overestimated (see discussion in Ref. [29]).

Fit to DIS data based on evolution equations performed in Ref. [78] also provided an evidence for rather strong antishadowing effect at  $x \approx 0.1$ . However, the fit employed an ad hoc assumption that gluons are shadowed at the low scale  $Q_0^2$  exactly as  $F_2(x, Q^2)$  what might be true only by accident. Besides, in the  $x$  distribution of antishadowing was shaped ad hoc too.

A similar magnitude of antishadowing has been found in the analysis [110] of data on  $Q^2$  dependence of nuclear to nucleon ratio of the structure func-

tions,  $F_2^A(x, Q^2)/F_2^N(x, Q^2)$ . However it was based on the leading order QCD approximation which is not well justified at these values of  $Q^2$ .

Although neither of these results seem to be reliable, similarity of the scale of the predicted effect looks convincing, and we included the antishadowing of gluons in our calculations. We use the shape of  $x_2$  dependence and magnitude of gluon enhancement from Ref. [78].

### 9.7 Comparison with available data and predictions for higher energies

The dynamics of  $J/\Psi$  suppression at energy  $800\text{ GeV}$  is rather complicated and includes many effects. Now we can apply more corrections to the dotted curve in Fig. 19 which involves only quark and gluon shadowing. Namely, inclusion of the energy loss effect and decay  $\chi \rightarrow J/\Psi \gamma$  leads to a stronger suppression depicted by the dashed curve. Eventually we correct this curve for gluon enhancement at  $x_2 \sim 0.1$  (small  $x_F$ ) and arrive at the final result shown by thick solid curve.

Since our calculation contains no free parameters we think that the results agree with the data amazingly well. Some difference in the shape of the maximum observed and calculated at small  $x_F$  may be a result of the used parameterization [78] for gluon antishadowing. We think that it gives only the scale of the effect, but neither the ad hoc shape, nor the magnitude should be taken literally. Besides, our calculations are relevant only for those  $J/\Psi$ s which originate from  $\chi$  decays which feed only about 40% of the observed ones.

At higher energies of RHIC and LHC, the effect of energy loss is completely gone and nuclear suppression must expose  $x_2$  scaling. Much smaller  $x_2$  can be reached at higher energies. Our predictions for proton-gold to proton-proton ratio is depicted in Fig. 22. One can see that at  $x_F > 0.1$  shadowing suppresses charmonium production by nearly an order of magnitude. We can also estimate the effect of nuclear suppression in heavy ion collisions assuming factorization,

$$R_{AB}(x_F) = R_{pB}(x_F) R_{pA}(-x_F) . \quad (135)$$

Our predictions for gold-gold collisions at  $\sqrt{s} = 200\text{ GeV}$  are shown by the bottom curve in Fig. 22. Since factorization is violated this prediction should be verified.

## 10 Summary

In these lectures, we presented several QCD processes related to production of heavy quarks at high energies. We describe all these reactions within the same approach, a light-cone color-dipole formalism. We highlighted the main advantages of this approach in comparison with the alternative description based on the standard QCD parton model. The color-dipole formalism does not involve any uncertain  $K$ -factors, takes care and calculates higher twist corrections, predicts nuclear effects. At the same time, this approach is restricted to the small- $x$  domain.

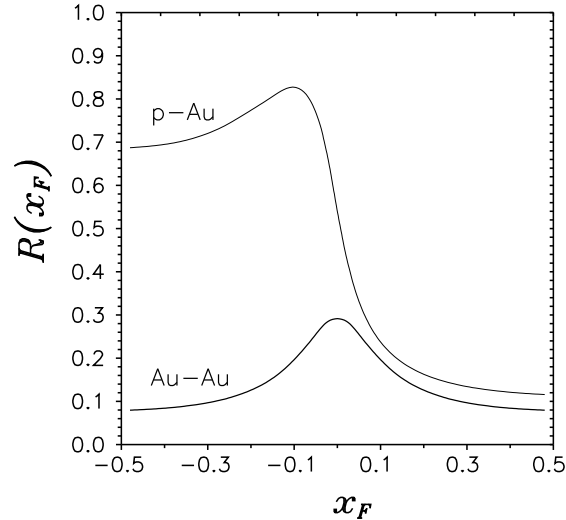


**Fig. 22.** Nuclear suppression of  $J/\Psi$  production in proton-gold collisions at  $\sqrt{s} = 200 \text{ GeV}$  as function of  $x_F$  (the upper curve) and in gold-gold collisions (bottom curve). Effects of quark and gluon shadowing and gluon antishadowing are included.

We started with the simplest process of diffractive production of charmonia off protons and nuclei. We made use of the best of our knowledge for charmonium wave functions and methods of their boosting to the light front. As a result, we arrived at a very good agreement with data, achieved without any adjustments. One of the key issues in reaching this agreement is inclusion of the Melosh spin rotation which substantially changes the production rates of  $J/\Psi$  and especially  $\Psi'$ . In particular, it solves the long standing problem of understanding photoproduction data for the  $\Psi'$  to  $J/\Psi$  ratio. These calculations also provided realistic predictions for charmonium-nucleon total cross sections.

We extended the study to charmonium photoproduction on nuclear targets aiming to study shadowing effects. Surprisingly, we found that higher twist shadowing which is neglected in parton model calculations, is the main source of shadowing, at least for foreseen energies. This shadowing effect is related to a nonzero separation of the produced  $c\bar{c}$  and vanishes in the limit of very heavy quarks. The leading twist shadowing, so called gluon shadowing, is related to higher Fock components of the photon containing gluons. It depends only logarithmically on the quark mass, but its onset is delayed to very high energies.

The next important process is hadroproduction of open heavy flavor. The color-dipole approach turns out to be quite effective even for a proton target due to well developed phenomenology for the dipole cross section fitted to HERA



data for  $F_2^p(x, Q^2)$ . Our predictions for open charm and beauty production well agrees with available data.

Higher twist quark shadowing for open charm hadroproduction off nuclei is a quite weak effect. However, we find large higher twist corrections to the leading twist gluon shadowing, which makes the latter process dependent. Gluon shadowing in open charm production is found to be stronger than in photoproduction of charmonium (and in DIS), but somewhat weaker than in the case of hadroproduction of charmonium. Our predictions for RHIC will be tested soon.

The last and most complicated case is hadroproduction of charmonia. We restricted ourselves to the simplest case of production of the  $P$ -wave  $\chi$  states. Like in photoproduction, we found a substantial higher twist shadowing, but much stronger leading twist gluon shadowing. For the first time we explained the steep  $x_F$  dependence of nuclear suppression of charmonia observed in the E772/866 experiments at Fermilab. Gluon shadowing is dramatically enhanced at the energies of RHIC and LHC and we predict very strong suppression of charmonia both for  $pA$  and  $AA$  collisions.

**Acknowledgments:** We are grateful to David Blaschke for his patience in encouraging us to write these lectures. Special thanks go to our collaborators Jörg Hüfner, Yuri Ivanov, Jen-Chieh Peng and Sasha Tarasov with whom the results presented here have been achieved. We thank the Institute for Nuclear Theory at the University of Washington for its hospitality during the workshop *The First Three Years of Heavy-ion Physics at RHIC*, where this work was completed. B.Z.K. is supported by the grant from the Gesellschaft für Schwerionenforschung Darmstadt (GSI), grant No. GSI-OR-SCH, and by the grant INTAS-97-OPEN-31696. J.R. is supported by the U.S. Department of Energy at Los Alamos National Laboratory under Contract No. W-7405-ENG-38.

## References

1. J. Hüfner, Y. P. Ivanov, B. Z. Kopeliovich and A. V. Tarasov, Phys. Rev. D **62**, 094022 (2000) [arXiv:hep-ph/0007111].
2. B. Kopeliovich, A. Tarasov and J. Hüfner, Nucl. Phys. A **696**, 669 (2001) [arXiv:hep-ph/0104256].
3. Y. P. Ivanov, B. Z. Kopeliovich, A. V. Tarasov and J. Hüfner, Phys. Rev. C **66**, 024903 (2002) [arXiv:hep-ph/0202216].
4. B. Z. Kopeliovich and A. V. Tarasov, Nucl. Phys. A **710**, 180 (2002) [arXiv:hep-ph/0205151].
5. J. Raufeisen and J. C. Peng, Phys. Rev. D **67**, 054008 (2003) [arXiv:hep-ph/0211422].
6. J. Raufeisen, J. C. Peng and G. C. Nayak, Phys. Rev. D **66**, 034024 (2002) [arXiv:hep-ph/0204095];  
B. Z. Kopeliovich, J. Raufeisen and A. V. Tarasov, Phys. Lett. B **503**, 91 (2001) [arXiv:hep-ph/0012035].
7. S. Gavin, P. L. McGaughey, P. V. Ruuskanen and R. Vogt, Phys. Rev. C **54**, 2606 (1996).

8. K. J. Eskola, V. J. Kolhinen and R. Vogt, Nucl. Phys. A **696**, 729 (2001) [arXiv:hep-ph/0104124].
9. L. V. Gribov, E. M. Levin and M. G. Ryskin, Nucl. Phys. B **188**, 555 (1981); Phys. Rept. **100**, 1 (1983);  
A. H. Mueller and J. w. Qiu, Nucl. Phys. B **268**, 427 (1986).
10. D. E. Kharzeev and J. Raufeisen, AIP Conference Proceedings, PASI 2002, Campos do Jordao, *New states of matter in hadronic interactions* Vol. 631, Issue 1, pp. 27-69 [arXiv:nucl-th/0206073].
11. C. Gerschel and J. Hüfner, Ann. Rev. Nucl. Part. Sci. **49**, 255 (1999) [arXiv:hep-ph/9802245];  
R. Vogt, Phys. Rept. **310**, 197 (1999).
12. T. Matsui and H. Satz, Phys. Lett. B **178**, 416 (1986).
13. A. B. Zamolodchikov, B. Z. Kopeliovich and L. I. Lapidus, JETP Lett. **33**, 595 (1981) [Pisma Zh. Eksp. Teor. Fiz. **33**, 612 (1981)].
14. B. Blaettel, G. Baym, L. L. Frankfurt and M. Strikman, Phys. Rev. Lett. **70**, 896 (1993);  
L. L. Frankfurt, A. Radyushkin and M. Strikman, Phys. Rev. D **55**, 98 (1997) [hep-ph/9610274].
15. B. Z. Kopeliovich, proc. of the workshop *Dynamical Properties of Hadrons in Nuclear Matter*, Hirscheegg, January 16 – 21, 1995, ed. by H. Feldmeyer and W. Nörenberg, Darmstadt, 1995, p. 102 (hep-ph/9609385).
16. S. Catani, M. Ciafaloni and F. Hautmann, Nucl. Phys. B **366**, 135 (1991);  
J. Kwiecinski, A. D. Martin and A. M. Stasto, Phys. Rev. D **56**, 3991 (1997) [arXiv:hep-ph/9703445];  
C. B. Mariotto, M. B. Gay Ducati and M. V. Machado, Phys. Rev. D **66**, 114013 (2002) [arXiv:hep-ph/0208155].
17. M. Abramowitz and I. A. Stegun (eds.), *Handbook of Mathematical Functions*, Dover Publications Inc., New York, NY, 1972.
18. A.H. Mueller, Nucl. Phys. B **558**, 285 (1999) [arXiv:hep-ph/9904404].
19. J. B. Kogut and D. E. Soper, Phys. Rev. D **1**, 2901 (1970).
20. J. D. Bjorken, J. B. Kogut and D. E. Soper, Phys. Rev. D **3**, 1382 (1971).
21. N. N. Nikolaev and B. G. Zakharov, J. Exp. Theor. Phys. **78**, 598 (1994) [Zh. Eksp. Teor. Fiz. **105**, 1117 (1994)].
22. G. Bertsch, S. J. Brodsky, A. S. Goldhaber and J. F. Gunion, Phys. Rev. Lett. **47**, 297 (1981).
23. S. J. Brodsky and A. H. Mueller, Phys. Lett. B **206**, 685 (1988).
24. E. A. Kuraev, L. N. Lipatov and V. S. Fadin, Sov. Phys. JETP **45**, 199 (1977) [Zh. Eksp. Teor. Fiz. **72**, 377 (1977)];  
I. I. Balitsky and L. N. Lipatov, Sov. J. Nucl. Phys. **28**, 822 (1978) [Yad. Fiz. **28**, 1597 (1978)].
25. V. S. Fadin and L. N. Lipatov, Phys. Lett. B **429**, 127 (1998);  
M. Ciafaloni and G. Camici, Phys. Lett. B **430**, 349 (1998).
26. A. Bialas, H. Navelet and R. Peschanski, Nucl. Phys. B **593**, 438 (2001) [arXiv:hep-ph/0009248].
27. H. I. Miettinen and J. Pumplin, Phys. Rev. D **18**, 1696 (1978).
28. K. Golec-Biernat and M. Wüsthoff, Phys. Rev. D **59**, 014017 (1999) [hep-ph/9807513]; Phys. Rev. D **60**, 114023 (1999) [hep-ph/9903358].
29. B. Z. Kopeliovich, A. Schäfer and A. V. Tarasov, Phys. Rev. D **62**, 054022 (2000) [arXiv:hep-ph/9908245].
30. M. G. Ryskin, R. G. Roberts, A. D. Martin and E. M. Levin, Z. Phys. C **76**, 231 (1997) [arXiv:hep-ph/9511228].

31. J. J. Aubert *et al.*, Phys. Rev. Lett. **33**, 1404 (1974);  
J. E. Augustin *et al.*, Phys. Rev. Lett. **33**, 1406 (1974).
32. J. Hüfner and B. Z. Kopeliovich, Phys. Lett. B **445**, 223 (1998) [arXiv:hep-ph/9809300].
33. B. Z. Kopeliovich and B. G. Zakharov, Phys. Rev. D **44**, 3466 (1991).
34. W. Lucha and F. F. Schoberl, Int. J. Mod. Phys. C **10**, 607 (1999) [arXiv:hep-ph/9811453].
35. E. Eichten, K. Gottfried, T. Kinoshita, K. D. Lane and T. M. Yan, Phys. Rev. D **17**, 3090 (1978) [Erratum-ibid. D **21**, 313 (1980)];  
E. Eichten, K. Gottfried, T. Kinoshita, K. D. Lane and T. M. Yan, Phys. Rev. D **21**, 203 (1980).
36. W. Buchmüller and S. H. Tye, Phys. Rev. D **24**, 132 (1981).
37. C. Quigg and J. L. Rosner, Phys. Lett. B **71**, 153 (1977).
38. A. Martin, Phys. Lett. B **93**, 338 (1980).
39. O. Benhar, B. Z. Kopeliovich, C. Mariotti, N. N. Nikolaev and B. G. Zakharov, Phys. Rev. Lett. **69**, 1156 (1992).
40. M. V. Terentev, Sov. J. Nucl. Phys. **24**, 106 (1976) [Yad. Fiz. **24**, 207 (1976)].
41. P. Hoyer and S. Peigne, Phys. Rev. D **61**, 031501 (2000).
42. K. Suzuki, A. Hayashigaki, K. Itakura, J. Alam and T. Hatsuda, Phys. Rev. D **62**, 031501 (2000) [arXiv:hep-ph/0005250].
43. H. J. Melosh, Phys. Rev. D **9**, 1095 (1974);  
W. Jaus, Phys. Rev. D **41**, 3394 (1990).
44. M. G. Ryskin, Z. Phys. C **57**, 89 (1993).
45. S. J. Brodsky, L. Frankfurt, J. F. Gunion, A. H. Mueller and M. Strikman, Phys. Rev. D **50**, 3134 (1994) [arXiv:hep-ph/9402283];  
L.L. Frankfurt, W. Koepf and M.I. Strikman, Phys. Rev. D **54** 3194 (1996).
46. J. Nemchik, N. N. Nikolaev, E. Predazzi and B. G. Zakharov, Z. Phys. C **75**, 71 (1997) [arXiv:hep-ph/9605231].
47. C. Adloff *et al.* [H1 Collaboration], Phys. Lett. B **483**, 23 (2000) [arXiv:hep-ex/0003020].
48. E401 Collab., M. Binkley *et al.*, Phys. Rev. Lett. **48** 73 (1982).
49. E516 Collab., B. H. Denby *et al.*, Phys. Rev. Lett. **52** 795 (1984).
50. J. Breitweg *et al.* [ZEUS Collaboration], Z. Phys. C **75**, 215 (1997) [arXiv:hep-ex/9704013].
51. J. Hüfner, B. Kopeliovich and A. B. Zamolodchikov, Z. Phys. A **357**, 113 (1997) [arXiv:nucl-th/9607033].
52. S. J. Brodsky and M. Karliner, Phys. Rev. Lett. **78**, 4682 (1997) [arXiv:hep-ph/9704379].
53. N. Armesto, A. Capella, A. B. Kaidalov, J. Lopez-Albacete and C. A. Salgado, arXiv:hep-ph/0304119.
54. B. Z. Kopeliovich, J. Raufeisen, A. V. Tarasov and M. B. Johnson, Phys. Rev. C **67**, 014903 (2003) [arXiv:hep-ph/0110221].
55. B. Z. Kopeliovich, J. Nemchik, N. N. Nikolaev and B. G. Zakharov, Phys. Lett. B **324**, 469 (1994) [arXiv:hep-ph/9311237].
56. B. Z. Kopeliovich, J. Raufeisen and A. V. Tarasov, Phys. Lett. B **440**, 151 (1998) [arXiv:hep-ph/9807211];  
J. Raufeisen, A. V. Tarasov and O. O. Voskresenskaya, Eur. Phys. J. A **5**, 173 (1999) [arXiv:hep-ph/9812398].
57. V.N. Gribov, Sov. Phys. JETP **29**, 483 (1969) [Zh. Eksp. Teor. Fiz. **56**, 892 (1969)].

58. B. Z. Kopeliovich, J. Raufeisen and A. V. Tarasov, Phys. Rev. C **62**, 035204 (2000) [arXiv:hep-ph/0003136].
59. N. N. Nikolaev, G. Piller and B. G. Zakharov, J. Exp. Theor. Phys. **81** (1995) 851 [Zh. Eksp. Teor. Fiz. **108** (1995) 1554] [arXiv:hep-ph/9412344]; Z. Phys. A **354**, 99 (1996) [arXiv:hep-ph/9511384].
60. P. Nason, S. Dawson and R. K. Ellis, Nucl. Phys. B **303**, 607 (1988).
61. P. Nason, S. Dawson and R. K. Ellis, Nucl. Phys. B **327**, 49 (1989) [Erratum-ibid. B **335**, 260 (1990)].
62. M.L. Mangano, P. Nason and G. Ridolfi, Nucl. Phys. B **373**, 295 (1992).
63. J. Bartels, K. Golec-Biernat and H. Kowalski, Phys. Rev. D **66**, 014001 (2002) [arXiv:hep-ph/0203258].
64. M. Glück, E. Reya and A. Vogt, Eur. Phys. J. C **5**, 461 (1998) [arXiv:hep-ph/9806404].
65. K. Kodama *et al.* [Fermilab E653 Collaboration], Phys. Lett. B **263**, 573 (1991); R. Ammar *et al.*, Phys. Rev. Lett. **61**, 2185 (1988); M. Aguilar-Benitez *et al.* [LEBC-EHS Collaboration], Z. Phys. C **40**, 321 (1988); G. A. Alves *et al.* [E769 Collaboration], Phys. Rev. Lett. **77**, 2388 (1996) [Erratum-ibid. **81**, 1537 (1998)]; S. Barlag *et al.* [ACCMOR Collaboration], Z. Phys. C **39**, 451 (1988).
66. K. Adcox *et al.* [PHENIX Collaboration], Phys. Rev. Lett. **88**, 192303 (2002) [arXiv:nucl-ex/0202002].
67. R. Vogt, arXiv:hep-ph/0203151.
68. A. Donnachie and P. V. Landshoff, Phys. Lett. B **296**, 227 (1992) [arXiv:hep-ph/9209205].
69. D. M. Jansen *et al.* [E789 Collaboration], Phys. Rev. Lett. **74**, 3118 (1995).
70. T. Alexopoulos *et al.* [E771 Collaboration], Phys. Rev. Lett. **82**, 41 (1999).
71. I. Abt *et al.* [HERA-B Collaboration], arXiv:hep-ex/0205106.
72. R. Bonciani, S. Catani, M. L. Mangano and P. Nason, Nucl. Phys. B **529**, 424 (1998) [arXiv:hep-ph/9801375]; N. Kidonakis, E. Laenen, S. Moch and R. Vogt, Phys. Rev. D **64**, 114001 (2001) [arXiv:hep-ph/0105041].
73. E789 Collaboration, M.J. Leitch *et al.*, Phys. Rev. Lett. **72** 2542 (1994).
74. E769 Collaboration, G.A. Alves *et al.*, Phys. Rev. Lett. **70** 722 (1993).
75. WA82 Collaboration, M. Adamovich *et al.*, Phys. Lett. B **284** 453 (1992).
76. NMC Coll., M. Arneodo *et al.*, Nucl. Phys. B **481** 23 (1996).
77. The E772 Collaboration, D.M. Alde *et al.*, Phys. Rev. Lett. **64** 2479 (1990).
78. K. J. Eskola, V. J. Kolhinen and P. V. Ruuskanen, Nucl. Phys. B **535**, 351 (1998) [arXiv:hep-ph/9802350]; K. J. Eskola, V. J. Kolhinen and C. A. Salgado, Eur. Phys. J. C **9**, 61 (1999) [arXiv:hep-ph/9807297].
79. M. Hirai, S. Kumano and M. Miyama, Phys. Rev. D **64**, 034003 (2001) [arXiv:hep-ph/0103208].
80. K.J. Eskola, H. Honkanen, V.J. Kolhinen, C.A. Salgado, hep-ph/0201256.
81. B. Z. Kopeliovich, J. Raufeisen and A. V. Tarasov, Phys. Lett. B **503**, 91 (2001) [arXiv:hep-ph/0012035]; M. A. Betemps, M. B. Gay Ducati and M. V. Machado, Phys. Rev. D **66**, 014018 (2002) [arXiv:hep-ph/0111473]; M. A. Betemps, M. B. Ducati, M. V. Machado and J. Raufeisen, arXiv:hep-ph/0303100.
82. S. J. Brodsky, A. Hebecker and E. Quack, Phys. Rev. D **55**, 2584 (1997) [arXiv:hep-ph/9609384].

83. B. Z. Kopeliovich, A. V. Tarasov and A. Schäfer, Phys. Rev. C **59**, 1609 (1999) [extended version in hep-ph/9808378].
84. M. B. Johnson, B. Z. Kopeliovich and A. V. Tarasov, Phys. Rev. C **63**, 035203 (2001) [arXiv:hep-ph/0006326];  
J. Raufeisen, Phys. Lett. B **557**, 184 (2003) [arXiv:hep-ph/0301052].
85. L. McLerran and R. Venugopalan, Phys. Rev. D **49**, 2233 (1994); **49**, 3352 (1994); **49**, 2225 (1994).
86. A.H. Mueller, *Parton saturation: an overview*, hep-ph/0111244.
87. L.D.Landau, I.Ya.Pomeranchuk, *ZhETF* **24** (1953) 505,  
L.D.Landau, I.Ya.Pomeranchuk, *Doklady AN SSSR* **92** (1953) 535, 735  
E.L.Feinberg, I.Ya.Pomeranchuk, *Doklady AN SSSR* **93** (1953) 439,  
I.Ya.Pomeranchuk, *Doklady AN SSSR* **96** (1954) 265,  
I.Ya.Pomeranchuk, *Doklady AN SSSR* **96** (1954) 481,  
E.L.Feinberg, I.Ya.Pomeranchuk, *Nuovo Cim. Suppl.* **4** (1956) 652.
88. A.H. Mueller, Nucl. Phys. **B335** (1990) 115; Nucl. Phys. B **558**, 285 (1999) [arXiv:hep-ph/9904404].
89. M. Arneodo, Phys. Rep. **240** 301 (1994).
90. M. B. Johnson *et al.* [FNAL E772 Collaboration], Phys. Rev. Lett. **86**, 4483 (2001) [arXiv:hep-ex/0010051];  
M. B. Johnson *et al.*, Phys. Rev. C **65**, 025203 (2002) [arXiv:hep-ph/0105195].
91. V.B. Berestetski, E.M. Lifshitz, and L.P. Pitaevski, *Relativistic Quantum Theory*. Clarendon Press, Oxford, 1971.
92. The NA3 Collaboration, J. Badier *et al.*, Z. Phys. **C20** 101 (1983).
93. The E537 Coll., S. Katsanevas *et al.*, Phys. Rev. Lett., **60** 2121 (1988).
94. The E866 Collaboration, M.J. Leitch *et al.*, Phys. Rev. Lett. **84** 3256 (2000).
95. The NA38 Collaboration, C. Baglin *et al.*, Phys. Lett. B **345** 617 (1995).
96. The NA50 Collaboration, M.C. Abreu *et al.*, Phys. Lett. B **477** 28 (2000).
97. M. Vaenttinen, P. Hoyer, S. J. Brodsky and W. K. Tang, Phys. Rev. D **51**, 3332 (1995) [arXiv:hep-ph/9410237].
98. E.L. Berger and D. Jones, Phys. Rev. **D23** 1521 (1981).
99. W. K. Tang and M. Vaenttinen, Phys. Rev. D **54**, 4349 (1996) [arXiv:hep-ph/9603266].
100. P. Hägler, R. Kirschner, A. Schäfer, L. Szymanowski and O. V. Teryaev, Phys. Rev. D **63**, 077501 (2001) [arXiv:hep-ph/0008316].
101. J. Hüfner and B. Kopeliovich, Phys. Rev. Lett. **76**, 192 (1996) [arXiv:hep-ph/9504379].
102. D. Kharzeev and H. Satz, Phys. Lett. B **356**, 365 (1995) [arXiv:hep-ph/9504397].
103. K. Ackerstaff *et al.* [HERMES Collaboration], Phys. Rev. Lett. **82**, 3025 (1999) [arXiv:hep-ex/9811011].
104. J. Hüfner, B. Kopeliovich and J. Nemchik, Phys. Lett. B **383**, 362 (1996) [arXiv:nucl-th/9605007].
105. K. Boreskov, A. Capella, A. Kaidalov and J. Tran Thanh Van, Phys. Rev. D **47** 919 (1993).
106. B.Z. Kopeliovich, *Dynamics and Phenomenology of Charmonium Production off Nuclei*, in proc. of the Workshop Hirschegg'97: QCD Phase Transitions', Hirschegg, Austria, January, 1997, ed. by H. Feldmeier, J. Knoll, W. Nörenberg and J. Wambach, Darmstadt, 1997, p. 281; hep-ph/9702365
107. B.Z. Kopeliovich and F. Niedermayer, *Nuclear screening in  $J/\Psi$  and Drell-Yan pair production*, JINR-E2-84-834, Dubna 1984, see the scanned version in KEK library:[http://www-lib.kek.jp/cgi-bin/img\\_index?8504113](http://www-lib.kek.jp/cgi-bin/img_index?8504113)

108. O.V. Kancheli, Sov. Phys. JETP Lett. **18** 274 (1973).
109. B. G. Zakharov, Phys. Atom. Nucl. **61**, 838 (1998) [Yad. Fiz. **61**, 924 (1998)]; [arXiv:hep-ph/9807540].
110. T. Gousset and H. J. Pirner, Phys. Lett. B **375**, 349 (1996) [arXiv:hep-ph/9601242].